Redox Biology 66 (2023) 102862

Contents lists available at ScienceDirect

Redox Biology

journal homepage: www.elsevier.com/locate/redox

Exacerbated response to oxidative stress in the Retinitis Pigmentosa *Cerkl*$^{KD/KO}$ mouse model triggers retinal degeneration pathways upon acute light stress

Rocío García-Arroyo [a,b,c], Elena B. Domènech [a,b,c], Carlos Herrera-Úbeda [a,b], Miguel A. Asensi [c,d], Cristina Núñez de Arenas [c,e,f], José M. Cuezva [c,e,f], Jordi Garcia-Fernàndez [a,b], Federico V. Pallardó [c,d], Serena Mirra [a,b,c,**], Gemma Marfany [a,b,c,*]

[a] Department of Genetics, Microbiology and Statistics, Universitat de Barcelona, Barcelona, Spain
[b] Institut de Biomedicina de la Universitat de Barcelona – Institut de Recerca Sant Joan de Déu (IBUB-IRSJD), Barcelona, Spain
[c] Centro de Investigación Biomédica En Red (CIBER) de Enfermedades Raras (CIBERER), ISCIII, Madrid, Spain
[d] Department of Physiology, University of Valencia-INCLIVA, Valencia, Spain
[e] Departament of Molecular Biology, Centro de Biología Molecular Severo Ochoa, Consejo Superior de Investigaciones Científicas-Universidad Autónoma de Madrid (CSIC-UAM), Madrid, Spain
[f] Instituto de Investigación Hospital 12 de Octubre, Madrid, Spain

ARTICLE INFO

Keywords:
CERamide kinase-like
Inherited retinal dystrophies
Oxidative stress
Light injury
Stress response
Retinal degeneration

ABSTRACT

The retina is particularly vulnerable to genetic and environmental alterations that generate oxidative stress and cause cellular damage in photoreceptors and other retinal neurons, eventually leading to cell death. *CERKL* (*CERamide Kinase-Like*) mutations cause Retinitis Pigmentosa and Cone-Rod Dystrophy in humans, two disorders characterized by photoreceptor degeneration and progressive vision loss. *CERKL* is a resilience gene against oxidative stress, and its overexpression protects cells from oxidative stress-induced apoptosis. Besides, CERKL contributes to stress granule-formation and regulates mitochondrial dynamics in the retina. Using the *Cerkl*$^{KD/KO}$ albino mouse model, which recapitulates the human disease, we aimed to study the impact of *Cerkl* knockdown on stress response and activation of photoreceptor death mechanisms upon light/oxidative stress. After acute light injury, we assessed immediate or late retinal stress response, by combining both omic and non-omic approaches. Our results show that *Cerkl* knockdown increases ROS levels and causes a basal exacerbated stress state in the retina, through alterations in glutathione metabolism and stress granule production, overall compromising an adequate response to additional oxidative damage. As a consequence, several cell death mechanisms are triggered in *Cerkl*$^{KD/KO}$ retinas after acute light stress. Our studies indicate that *Cerkl* gene is a pivotal player in regulating light-challenged retinal homeostasis and shed light on how mutations in *CERKL* lead to blindness by dysregulation of the basal oxidative stress response in the retina.

1. Introduction

The retina is daily exposed to bright light, which coupled with its own highly active and energy-demanding metabolism, ultimately generating oxidative damage, and facilitate the formation of reactive oxygen species (ROS). The accumulation of ROS alters the composition and structure of retinal nucleic acids, proteins, and lipids, eventually compromising the homeostasis and health of photoreceptors and other retinal neurons [1]. Thus, the retina requires accurate stress resilience mechanisms and compensating antioxidant responses to ensure cell survival and physiological homeostasis [2].

In the retina, the resident microglia as well as the macroglia, play a pivotal role in counteracting stress stimuli by orchestrating defensive actions, tissue repair and immunoregulation. Their activation is characterized by proliferation and morphological changes, in a process called gliosis [3,4]. At the intracellular level, the endoplasmic reticulum and mitochondria are key hubs involved in sensing oxidative stress [5]. In addition, there are different specific protective mechanisms against

* Corresponding author. Department of Genetics, Microbiology and Statistics, Universitat de Barcelona, Barcelona, Spain.
** Corresponding author. Department of Genetics, Microbiology and Statistics, Universitat de Barcelona, Barcelona, Spain.
E-mail addresses: serena.mirra@ub.edu (S. Mirra), gmarfany@ub.edu (G. Marfany).

https://doi.org/10.1016/j.redox.2023.102862
Received 1 August 2023; Received in revised form 22 August 2023; Accepted 25 August 2023
Available online 28 August 2023
2213-2317/© 2023 The Authors. Published by Elsevier B.V. This is an open access article under the CC BY-NC-ND license (http://creativecommons.org/licenses/by-nc-nd/4.0/).

stress, such as the regulation of glutathione metabolism balance [6] and the formation of mRNA stress-granules and P-bodies, two structures that protect non-translated mRNAs after damaging stimuli [7,8]. Dysregulation, impairment or chronic activation of the antioxidant mechanisms in the retina is at the basis of many retinal neurodegenerative disorders.

Mutations in *CERKL* cause two related but distinct inherited retinal dystrophies: Retinitis Pigmentosa and Cone-Rod Dystrophy, both of them causing irreversible attrition of photoreceptor cells, which eventually results in total blindness [9–12]. Previous studies have postulated *CERKL* as a resilience gene against oxidative stress in the retina by participating in autophagy [13–15], apoptosis inhibition [16,17], mitochondrial dynamics and function regulation [15,18,19], and stress granules formation [20]. On the latter, CERKL has been shown to interact with different proteins that compose mRNA stress-granules and P-bodies [20]. Importantly, *CERKL* downregulation affects mitochondrial homeostasis and impairs mitochondrial response against oxidative stress, while *CERKL* overexpression protects cells from acute oxidative stress [18]. Nevertheless, the specific pathogenesis mechanisms of *CERKL* mutations have not been fully determined yet.

To thoroughly understand the molecular role and mechanisms in which CERKL is involved, and since the human retina of patients cannot be biochemically studied nor challenged, we studied a knockdown/knockout *Cerkl* mouse model (*Cerkl*$^{KD/KO}$ or *KD/KO*). This model exhibits a remaining expression of 18% of some *Cerkl* isoforms, as those expressed from the proximal promoter are completely ablated [21]. Patients carry many different combinations of *CERKL* mutations, many as compound heterozygotes, with one allele producing a truncated or no protein at all (mRNA containing premature STOP codons are degraded by nonsense mediated decay) and other alleles that alter some but not all CERKL protein isoforms. In this context, our compound heterozygote mouse *KD/KO* model is genetically very similar to the mutations identified in human patients, and more relevant to our work, the slow progression of the retinal degeneration in our *KD/KO* retinas mimics that shown in human patients carrying *CERKL* mutations, being the final outcome retinal neurodegeneration and vision loss [21].

Light stress treatment has been largely employed to induce oxidative stress and thus promote retinal neurodegeneration to study the molecular mechanisms evoking this process in retinal dystrophies [22,23]. Taking advantage of the *KD/KO* mouse model, the main goal of this work has been the characterization of the response to acute light-induced stress upon *Cerkl* downregulation by exposing *KD/KO* albino mice to light stress and evaluating different parameters through RNA sequencing (RNA-Seq), protein and metabolites analyses as an early response to stress injury, as well as retinal morphology and remodelling two weeks after light stress damage. Our data revealed that *KD/KO* retinas show exacerbated oxidative stress response in basal conditions and thus, could not respond properly to light stress due to the impairment of different antioxidant mechanisms, such as glutathione balance and PABP mRNA-stress granules formation. Subsequently, several cell death pathways were triggered in *KD/KO* retinas resulting in neurodegeneration and retinal remodelling. Our results offer a highly detailed characterization of the basal REDOX status and oxidative/light stress response in the *Cerkl*$^{KD/KO}$ mouse model, with the final aim to identify altered actionable antioxidant pathways as key targets for potential therapeutic intervention.

2. Materials and methods

2.1. Animal handling

WT/WT and *KD/KO* albino mice (B6(Cg)-Tyrc-2J/J) were bred and housed in the animal research facilities at the University of Barcelona. Animals were provided with food and water ad libitum and maintained in a temperature-controlled environment in a 12/12 h light–dark cycle. All animal handling and assays were performed according to the ARVO statement for the use of animals in ophthalmic and vision research, as well as the regulations of the Ethical Committee for Animal Experimentation (AEC) of the Generalitat de Catalunya (protocol C-449/18 (animal handling) and protocol C-220/18 (light stress assays)), according to the European Directive 2010/63/EU and other relevant national guidelines. Each cohort (genotype and condition) had equivalent proportion of male and female mice, as autosomal recessive retinitis pigmentosa affects similarly both biological sexes.

2.2. Genomic DNA and genotyping by PCR

DNA for genotyping was extracted from ear punches. Primers for genotyping and PCR conditions were described in Ref. [21].

2.3. Light-stress treatment

Light stress experiments were performed on albino adult mice (4–6-months-old), where retinas are more sensitive to light injury due to the absence of pigmenti in the retinal pigment epithelium (RPE). Animals were anesthetized using a mixture of Ketamine (100 ng/kg)/Xylacine (10 ng/kg). One eye was covered to avoid the light insult (control) and the other was treated with a drop of 10 mg/mL cyclopentolate to dilate the pupil prior 3000-lux white light exposition for 1 h. At the end of the treatment, mice were immediately sacrificed to obtain the retinal tissue for the stress-early response study. On the other hand, for the stress-late response study, both eyes of the same mouse were subjected to light stress (3000 lux for 1 h). Two weeks after treatment, mice were sacrificed to obtain the retinal tissue.

2.4. Primary ganglion cell culture

Coverslips were freshly coated with 60 μL of poly-ornithine (Sigma Aldrich, Saint Louis, Missouri, USA), air dried and subsequently washed with MilliQ water. A drop of 10 μg/mL Laminin (Roche, Saint Louis, Missouri, USA) in complete neurobasal medium (Neurobasal™-A medium, Thermo Fisher Scientific, Waltham, MA, USA) supplemented with 0.06% D-Glucose, 0.0045% $NaHCO_3$, 1 mM L-Glutamine and 1% Penicillin/Streptomycin was added on pre-treated coverslips and incubated overnight at 37 °C. After three washes with complete neurobasal medium, coverslips were used for primary RGCs culture. E16 mouse retinas (3 animals per genotype) were dissociated using the Neural Tissue Dissociation Kit (Miltenyi Biotec, Bergisch, Gladbach, Germany) following the manufacturer's instructions with minor modifications. In brief, after Enzyme mix 2 incubation, 2 vol of complete neurobasal medium were added for gentle dissociation with the pipette. Cells were pelleted by 5 min centrifugation at 0.3 rcf and resuspended in complete neurobasal medium. Approximately 100000 cells/well were seeded onto coated coverslips in a 24 well/plate. Neuronal supplements and factors were added: 1 × B27 (Invitrogen, Carlsbad, California, USA), 5 μM Forskolin (Sigma Aldrich, Saint Louis, Missouri, USA), 50 ng/mL Human BDNF (Peprotech, Rock Hill, NJ, USA), 20 ng/mL Rat CNTF (Peprotech, Rock Hill, NJ, USA). RGCs at 7 DIV were subjected to oxidative stress by treatment with 0.5 mM sodium arsenite for 45 min. Afterwards, cells were fixed with 4% PFA for 20 min, washed 3 times with 1 × PBS and cryoprotected (30% Glycerol, 25% Ethyleneglycol and 0.1 M PBS) for further experiments.

2.5. Immunofluorescence, confocal microscopy, and colocalization analysis

In immunocytochemistry experiments, cells were blocked using 2% sheep serum and 0,3% Triton-X-100 (St. Louis, MO, USA) in 1 × PBS during 1 h at RT. Subsequently, cells were incubated with primary antibodies overnight at 4 °C in blocking solution. Primary antibodies used were the following: CERKL2 (1:200, in house, [21]), CERKL5 (1:100, in house, [21]), PABP-488 (1:50, sc-166381 AF488, Santa Cruz Biotechnology, Dallas, TX, USA). After three washes with 1 × PBS, cells were

incubated with the secondary antibody Alexa Fluor 568 anti-Rabbit IgG (1:400, A-11011, Thermo Fisher Scientific) in blocking solution during 1 h at RT. Nuclei were stained using DAPI (1:1000, 10236276001, Roche Diagnostics, Indianapolis, IN, USA) and after rinsing with 1 × PBS (3 × 5 min), samples were mounted using Mowiol 4–88 (Merck, Darmstadt, Germany).

For immunohistochemistry (IHC) of retinas, adult albino mice eyes were fixed overnight at 4 °C with 4% PFA, incubated with 30% sucrose overnight and embedded in OCT (ANAME, Quijorna, Madrid, Spain). Cryosections (12 μm) were collected and kept frozen at −80 °C until used. For IHC, cryosections were air-dried for 10 min, rehydrated with 1 × PBS, permeabilized using 0.5% Triton X-100 for 15 min and blocked in blocking solution (1 × PBS containing 10% Normal Goat Serum and 0,3% Triton X-100) for 1 h at RT. Primary antibody incubation was performed overnight at 4 °C in blocking solution. After three rinses with 1 × PBS (10 min each) cryosections were incubated for 1 h at RT with the corresponding secondary antibodies conjugated to a fluorophore. Finally, the slides were washed with 1 × PBS (3 × 10 min) and coverslipped with Mowiol 4–88 (Merck, Darmstadt, Germany). Primary antibodies and dilutions used were: RPE65 (1:500, sc-390787, SantaCruz Biotechnology), PABP (1:200, ab21060, Abcam), mouse anti-GFAP (1:300, MAB360, Millipore), Cone Arrestin (AB15282, Millipore), Phospho S358 MLKL (1:100, ab187091, Abcam), Bassoon (1:300, GTX13249, GeneTex), Cryaa (1:200, ab5595, Abcam), Crybb2 (1:200, sc-376006, SantaCruz Biotechnology). Secondary antibodies and dilutions used were the following: Alexa Fluor 488 anti-Rabbit IgG (1:400, A-11070, Thermo Fisher Scientific), Alexa Fluor 568 anti-Mouse IgG (1:400, A-11004, Thermo Fisher Scientific), DAPI (1:1000, Roche Diagnostics, Indianapolis, IN, USA).

Images were obtained in high-resolution microscopy (THUNDER Imager Live Cell & 3D Cell Culture & 3D Assay, Leica Microsystems, Wetzlar, Germany) and confocal microscopy (Zeiss LSM 880, Thornwood, NY, USA). Image analyses were performed using ImageJ (FIJI) software (National Institutes of Health, Bethesda, MD, USA). In this study, image intensity is considered proportional to the concentration of protein so, in order to provide a relative quantitative comparison, all the images were normalized to the same dynamic range. For analysis of total concentration of protein, the threshold value was adjusted to select the whole area of interest (e.g., the RPE) with signal, then the integrated density values were corrected using the CTCF formula (CTCF =Integrated Density – (Area of selected cell X Mean fluorescence of background readings)). Regarding the granules analysis, the threshold value was set to show only the brighter spots coming from the stress granules to further analyze the individual particles.

2.6. RNA isolation from mouse retinas and RNA-Seq

Three retinas per genotype and condition were homogenized using a Polytron PT1200E homogenizer (Kinematica, AG, Lucerne, Switzerland). Total RNA was isolated using the RNeasy mini kit (Qiagen, Germantown, MD), following the manufacturer's instructions with minor modifications (treatment with DNAse I during 1 h). Total RNA was quantified by Qubit® RNA BR Assay kit (Thermo Fisher Scientific) and the RNA integrity was estimated by using RNA 6000 Nano Bioanalyzer 2100 Assay (Agilent).

RNA-Seq libraries were prepared with KAPA Stranded mRNA-Seq Illumina® Platforms Kit (Roche) following the manufacturer's recommendations. Briefly, 100–300 ng of total RNA were used for poly-A fraction enrichment with oligo-dT magnetic beads, following mRNA fragmentation by divalent metal cations at high temperature. Strand specificity was achieved during the second strand synthesis performed in the presence of dUTP instead of dTTP. Blunt-ended double stranded cDNA was 3′adenylated and Illumina platform compatible adaptors with unique dual indexes and unique molecular identifiers (Integrated DNA Technologies) were ligated. The ligation product was enriched with 15 PCR cycles and the final library was validated on an Agilent 2100 Bioanalyzer with the DNA 7500 assay. The libraries were sequenced on HiSeq 4000 (Illumina) with a read length of 2x76bp+8bp+8bp using HiSeq 4000 SBS kit (Illumina) and HiSeq 4000 PE Cluster kit (Illumina), following the manufacturer's protocol for dual indexing. Image analysis, base calling and quality scoring of the run were processed using the manufacturer's software Real Time Analysis (RTA 2.7.7). RNA-Seq libraries and sequencing initial analysis were performed in the CNAG (Centro Nacional de Análisis Genómico, Barcelona). Differential expression analysis and heatmaps from RNA-Seq data were performed as in Ref. [15]. Gene Ontology (GO) Biological Process enrichment analysis was performed using Enrichr web server (https://maayanlab.cloud/Enrichr/) [24–26]. Gene pathway and functional clustering analyses were performed using GeneAnalytics™ (geneanalytics.genecards.org) and iDEP1.1 software [27]. The complete list of the RNA-Seq analysed genes is in the RNA-Seq Supplementary Data.

2.7. Western blotting

Adult retinas were lysed in RIPA buffer [50 mM Tris, pH 7.4, 150 mM NaCl, 1 mM EDTA, 1% NP-40, 0.25% Na-deoxycholate, protease inhibitors (Complete; Mini Protease Inhibitor Cocktail Tablets; Roche)] containing phosphatase inhibitors. Proteins were analysed by SDS-PAGE and transferred onto nitrocellulose membranes, which were blocked with 5% non-fat dry milk in 1 × PBS containing 0.1%Tween 20 and incubated overnight at 4 °C with primary antibodies. After incubation with horseradish peroxidase-labeled secondary antibodies for 1 h at room temperature, immunodetection was developed using the ECL system (Lumi-Light Western Blotting Substrate, Roche). Images were acquired by ImageQuant™ LAS 4000 mini Image Analyzer (Fuji-film) and quantified using ImageJ software. α-TUBULIN or GAPDH loading controls were used to normalize protein values. The primary antibodies were the following: GSR (1:1000, 18257-1-AP, Proteintech), GPX4 (1:1000, 52455, Cell Signaling Technology), Caspase-7 p11 (1:1000, PA5-90312, Thermo Fisher Scientific), FTH1 (1:1000, 4393, Cell Signaling Technology), KEAP1 (1:1000, 8047, Cell Signaling Technology), TUBULIN (1:1000, T5168, Sigma), GAPDH (1:1000, ab8245, Abcam). The secondary antibodies were: HRP-labeled anti-mouse (1:2000, A5906, Sigma) and anti-rabbit (1:2000, NA934-100UL, GE Healthcare).

2.8. Retinal explants and ROS-Glo H_2O_2 assay

Eyes were enucleated from adult mice and dissected in 1 × PBS containing 1% penicillin/streptomycin. Retinas were obtained after an incision in the pupil, cutting through the ora serrata and pulling from the posterior part of the eye. Then, 3 patches per retina were collected and cultured for 24 h in cell culture inserts (PICM03050, Millipore, Darmstadt, Germany) floating inside 6-multiwell plates containing retinal explant complete medium (Neurobasal™-A medium (Thermo Fisher Scientific, Waltham, Massachusetts, USA) supplemented with 0.06% D-Glucose, 0.0045% $NaHCO_3$, 1 mM L-Glutamine, 1% Penicillin/Streptomycin and 1 × B27 (Invitrogen, Carlsbad, CA, USA)). A total of 8 patches from 4 retinas per genotype were treated with 0.5 mM sodium arsenite for 24 h to perform oxidative stress treatment. Afterwards, all patches were distributed onto a 96-multiwell white plate (Greiner, Vienna, Austria) and ROS-Glo H_2O_2 Assay (Promega, Madison, WI, USA) was performed following the manufacturer's instructions.

2.9. Glutathione metabolism determination

Five retinas per genotype and condition were analysed. Reduced glutathione (GSH), oxidized glutathione (GSSG), homocysteine and γ-glutamyl cysteine levels were determined as follows: each retina was homogenized in 100 μL of PBS-N-Ethylmaleimide (NEM) buffer (5 mM). To induce protein precipitation, perchloric acid was added at 4% final concentration, and samples were centrifuged at 10,000 rpm, 15 min at

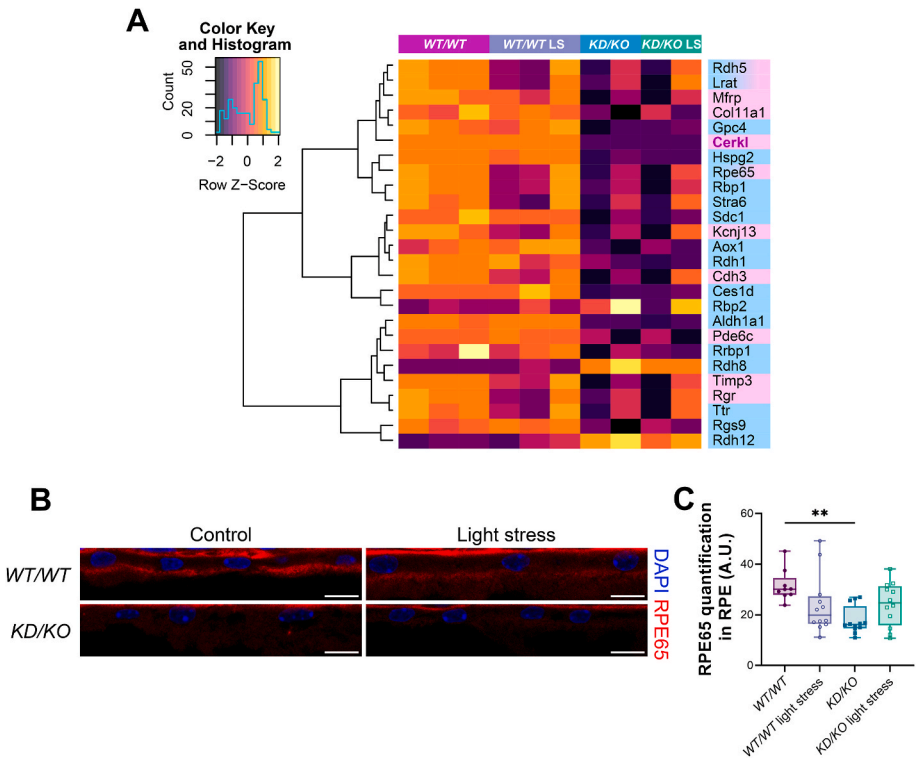

Fig. 1. Genes associated to inherited retinal dystrophies (IRDs) and phototransduction/visual cycle showed differential expression in *KD/KO* compared to *WT/WT* retinas (**A**) Heatmap with hierarchical clustering of differentially expressed genes associated with IRD genes (in pink) and phototransduction/visual cycle genes (in blue) in both control and light-stress (LS) conditions. (**B**) *RPE65* transcript and protein levels are significantly decreased in *KD/KO* retinal pigment epithelium (RPE) cells. Representative confocal images of RPE65 immunodetection (red) and nuclei staining (DAPI, in blue) from *WT/WT* and *KD/KO* RPE in control and under light-stress conditions (scale bar: 10 μm). Quantification of RPE65 signal intensity shown in (**C**), solely in the area of interest, reveals a significant decrease in *KD/KO* compared to *WT/WT* RPE. n = 12 ROIs from 4 animals per genotype and condition ** *p-value* ≤ 0.01. (For interpretation of the references to colour in this figure legend, the reader is referred to the Web version of this article.)

4 °C. Supernatants were transferred to a new tube for analysis and pellets were resuspended in 100 μL of NaOH (1 M) to obtain the total protein content using the BCA Protein Assay Kit (ThermoScientific, MA, USA). Then, metabolites of the transulfuration pathway were analysed by UPLC-MS/MS as described in Ref. [28]. Data were normalized by grams of total protein content.

2.10. Reverse phase protein in-house microarrays (RPPM)

Five retinas per genotype and condition were collected from adult albino *WT/WT* and *KD/KO* mice into liquid nitrogen right after light-induced stress treatment and subsequently lysed in 90 μL of Tissue Protein Extraction Reagent (T-PER, 78501, ThermoFisher Scientific) containing a cocktail of protease (Roche) and phosphatase (Sigma) inhibitors. Following protein extraction, samples were centrifuged at 15,000 g for 30 min at 4 °C. The RPPM technique was used for quantification of steady-state protein levels in the biopsies as recently described in detail [29–31]. Only monospecific antibodies recognizing the expected protein in cellular lysates were included in RPPM studies. Protein extracts from mouse retinas were diluted in PBS to a final protein concentration of 0.5 μg/μL before printing. Serially diluted protein extracts (0–1.5 μg/μL) derived from C2C12 mouse myoblast cells were prepared to assess printing quality and the linear response of protein recognition by the antibodies used [29]. Standard curves of BSA (0–2 μg/μl) and mouse IgGs (1–30 ng/μl) were also prepared as internal negative and positive controls, respectively. Approximately, 1.5 nL of each sample was spotted in triplicate onto nitrocellulose-coated glass slides (ONCYTE® SuperNOVA 8 pad—Grace Bio-Labs, 705118, Oregon, USA) using a iTWO-300P pico system printer (M2-Automation, Inc., Idaho, USA) equipped with a Piezo Driven Micro-Dispenser (PDMD) 30–150 pL at constant chamber humidity (RH 52%) and temperature (16 °C), and plate temperature (10 °C). After printing, arrays were allowed to dry and further blocked in Super G Blocking Buffer (10501, Grace Biolabs, Madrid, Spain). After, the arrays were incubated overnight at 4 °C with the indicated dilutions of the primary antibodies. After incubation, the arrays were washed with PBS-T and further incubated with goat anti-mouse or goat anti-rabbit highly cross-adsorbed antibodies conjugated with CF™ 647 (1:500, SAB4600183–SAB4600185, Sigma Aldrich, Madrid, Spain). Pads incubated directly with secondary antibodies and with 0.0001% Fast Green FCF (F7252, Sigma Aldrich, Madrid, Spain) were used to evaluate potential unspecific binding to non-masked mouse IgGs and the total protein amount present in the spotted samples, respectively. Microarrays were scanned using Typhoon 9410 scanner (GE Healthcare, Inc. Madrid, Spain). The mean fluorescent intensity of the spots was measured using GenePix® Pro 7 (USA) and normalized relative to the protein amount contained in the sample obtained from the FCF stained pad. After quantification, the relative fluorescent intensity was converted into arbitrary units of expressed protein/ng of protein in the extract using as standard the linear plot of the C2C12 cell line [29,30].

2.11. Statistical analyses

Statistical analyses were performed using 1-way and 2-way ANOVA tests performing multiple comparison analysis. When data did not follow a normal distribution, Kruskal-Wallis test was used to determine statistical significance. ROUT test was used to determine statistical outliers (Q = 0.5%). Calculations were performed with GraphPad Prism statistical software, version 9. N is shown at each Figure legend. Statistical significance was set with a value of $p \leq 0.05$, (*$p \leq 0.05$, **$p \leq 0.01$, ***$p \leq 0.005$, ****$p \leq 0.001$). Data were expressed as min to max boxplots showing all points.

3. Results

3.1. RNA-Seq analysis revealed differentially expressed genes associated with retinal dystrophies and phototransduction/visual cycle in KD/KO retinas

Preceding research has associated CERKL protein to stress resilience and mitochondrial dynamics regulation, but its contribution to specific oxidative stress pathways still needs further investigation. In this study,

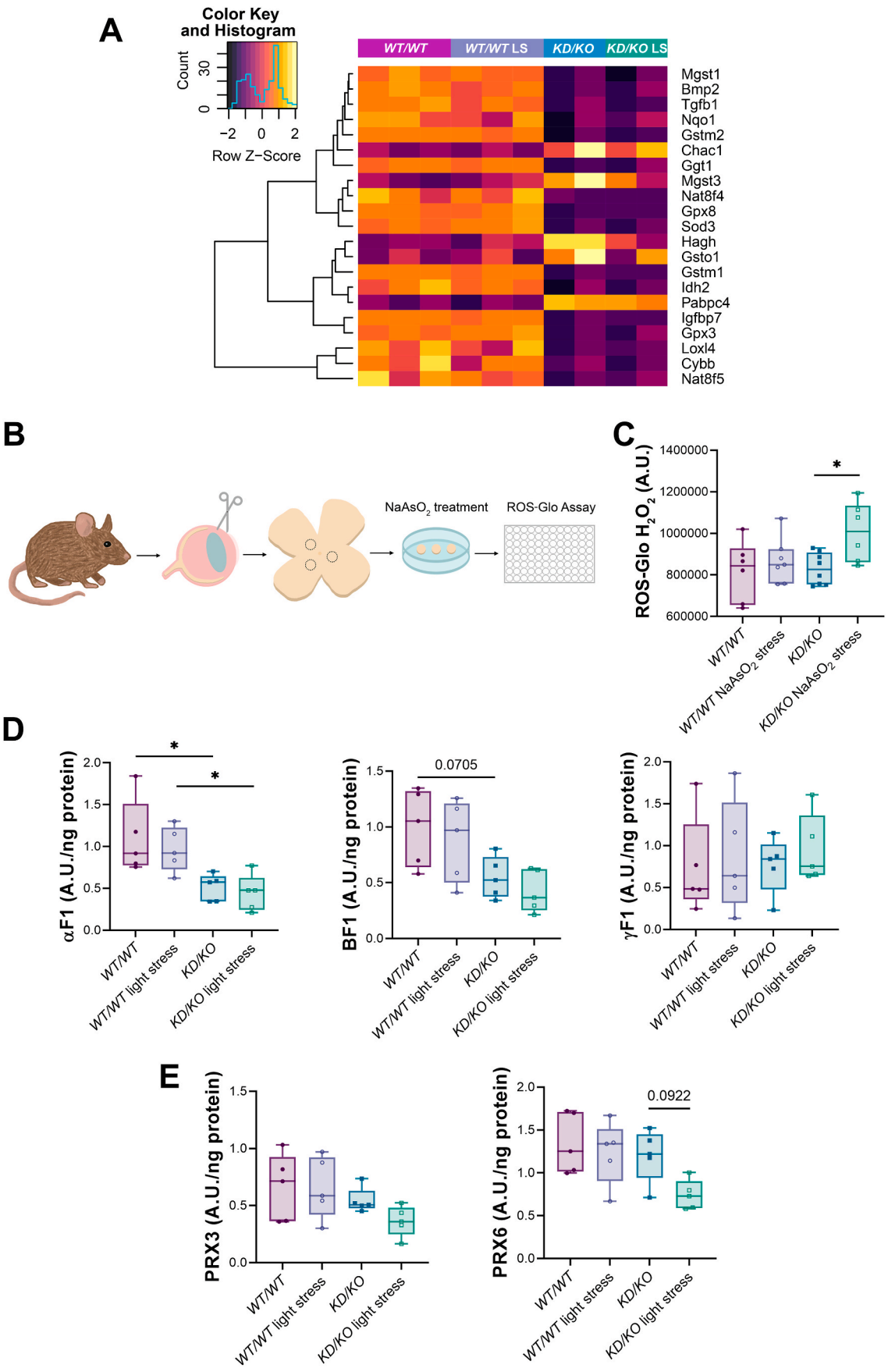

(caption on next page)

Fig. 2. Mitochondrial metabolism and antioxidant mechanisms are diminished in *KD/KO* retinas. (**A**) Heatmap with hierarchical clustering of differentially expressed genes associated with antioxidant responses. (**B**) Schematic representation of the assay including retinal patches obtention, sodium arsenite treatment and ROS-Glo H_2O_2 Assay. (**C**) Measurement of H_2O_2 levels by ROS-Glo H_2O_2 Assay reveals a significant increase in *KD/KO* retinal explants upon oxidative stress treatment. n = 6–8 retinal patches from 4 retinas per genotype and condition. (**D**) Alterations in the levels of different ATP synthase subunits in *KD/KO* retinas. Quantification of αF1, βF1 and γF1 proteins using reverse phase protein microarrays (RPPM). n = 5 animals per genotype and condition. (**E**) *KD/KO* retinas display a tendency to lower protein levels of PRX3 and PRX6 by means of microarray quantification. n = 5 animals per genotype and condition. * *p-value* ≤ 0.05. (Complementary data in Supplementary Fig. 3).

we aimed to determine CERKL role in the retina in response to acute light-stress insult. Retinas from *WT/WT* and *KD/KO* albino mice were exposed to 3000-lux white light for 1 h and assessed immediately after by RNA sequencing (RNA-Seq) analysis to explore their transcriptomic landscape in response to the light-stress treatment, as a first undirected wide approach. We identified a large set of differentially expressed (DE) genes between the assessed samples. A threshold of $\log_2$ Fold Change ±0.5 was set to distinguish between up- and downregulated genes between genotypes and conditions (Supplementary Figure 1). Notably, the more outstanding differences were found between genotypes rather than

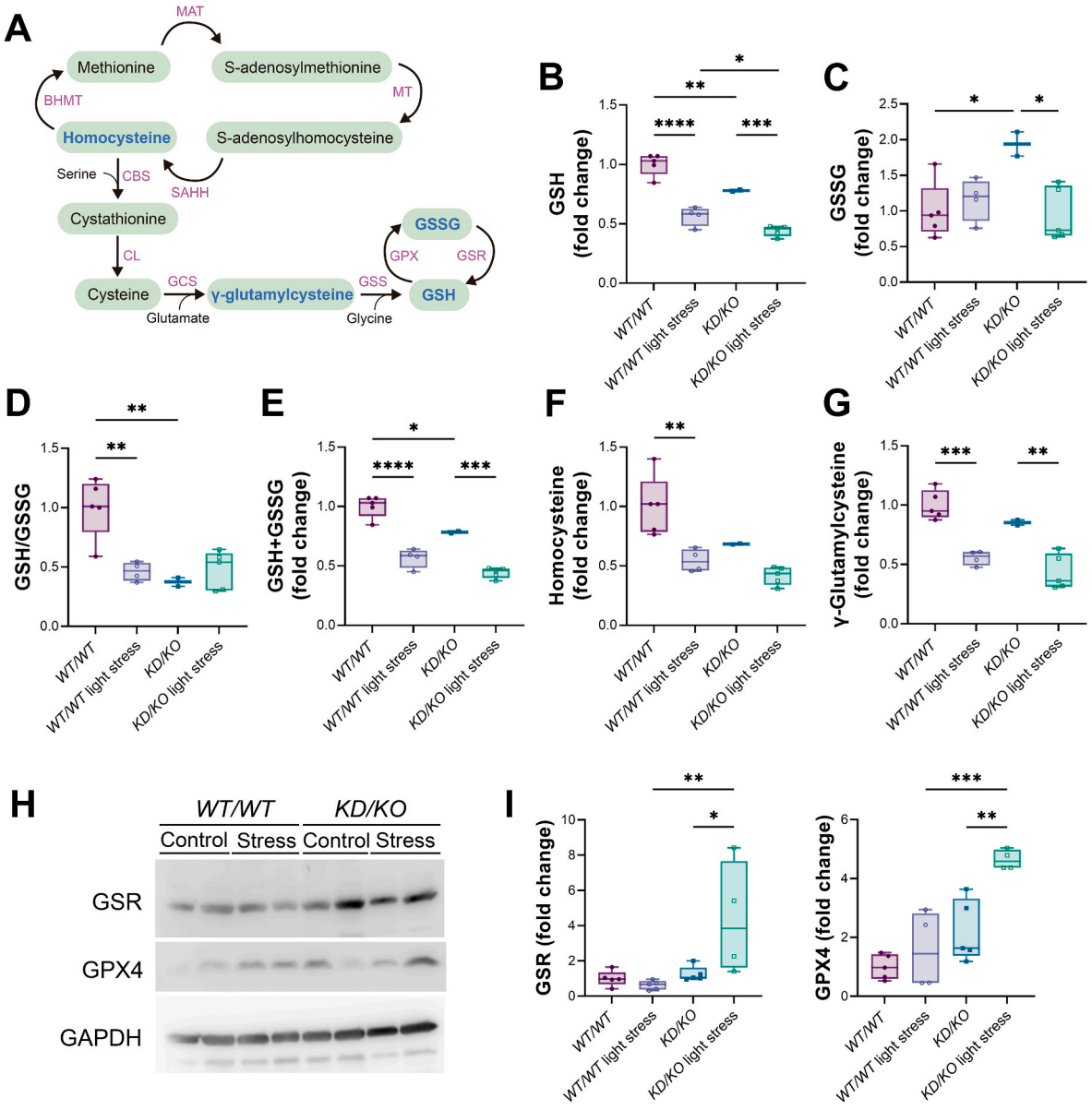

Fig. 3. Glutathione metabolism alteration in *KD/KO* retinas. (**A**) Schematic representation of glutathione metabolism and synthesis pathway (enzymes in purple). Metabolites altered in *KD/KO* retinas are highlighted in blue. (**B–I**) Glutathione metabolism and synthesis pathways are impaired in *KD/KO* retinas. (**B-E**) Quantification of the reduced (GSH) and oxidized (GSSG) forms of glutathione, as well as the GSH/GSSG ratio and total quantity of glutathione (GSH + GSSG) in *WT/WT* and *KD/KO* retinas in both control and light-stress conditions. (**F, G**) Measurement of homocysteine and γ-glutamylcysteine, precursors for the synthesis of glutathione, in *WT/WT* and *KD/KO* retinas in both control and light-stress treatment. n = 2–5 animals per genotype and condition. (**H, I**) GSR and GPX4 protein levels are significantly augmented in *KD/KO* retinas upon light-stress insult. (**H**) Representative Western-blot of GSR, GPX4 and GAPDH (as loading control) on retinal homogenates from *WT/WT* and *KD/KO* retinas in both control and light-stress conditions. (**I**) Quantification of GSR and GPX4 protein levels normalized with GAPDH levels. n = 4–5 animals per genotype and condition. * *p-value* ≤ 0.05, ** *p-value* ≤ 0.01, *** *p-value* ≤ 0.005, **** *p-value* ≤ 0.001. (Complementary data in Supplementary Fig. 4). (For interpretation of the references to colour in this figure legend, the reader is referred to the Web version of this article.)

between control/light-stress conditions. Besides, when analysing per genotypes, the number of downregulated genes in *KD/KO* retinas was approximately 5-fold higher than that of upregulated genes. Focusing on the upregulated genes in *KD/KO* in basal conditions, we observed a slight decrease in the levels of some genes when these retinas were subjected to light-stress insult (Supplementary Figure 1, upper panel).

Taking advantage of the "omic" data obtained by RNA-Seq, we identified many dysregulated cellular pathways. Notably, approximately 50% of all the upregulated Gene Ontology (GO) Biological Processes (32/75) in the *KD/KO* versus *WT/WT* retinas are directly related to stress response and pro-inflammatory pathways (Supplementary Table 1). In contrast, more than 60% of the downregulated GO Biological Processes (51/75) relate to organ development and differentiation pathways, including ocular development, visual cycle and sensory perception (Supplementary Table 2). Taken together, these data confirm that *KD/KO* retinas show both alteration of stress responses and dysregulation of homeostasis mechanisms.

We then concentrated on the different clusters of genes specifically involved in maintaining retinal function. One of these DE gene clusters was particularly interesting because the genes were related to inherited retinal dystrophies, IRDs (e.g., *Rpe65*, *Timp3*, *Mfrp*) (Fig. 1A, in pink) and/or implicated in the phototransduction/visual cycle process (e.g., *Lrat, Rdh12, Hspg2*, *Rdh1*, *Rgs9*) (Fig. 1A, in blue). As expected, in the retinal disorder-related gene cluster, *Cerkl* stands out by its highly decreased expression in *KD/KO* retinas (Fig. 1A, highlighted in purple). Of note, light stress did not increase the expression of *Cerkl* in the wild-type retinas, indicating that it is very stable transcriptionally and its involvement in stress might be post-translationally regulated, as suggested in Ref. [18].

Interestingly, most of these ocular-associated genes were downregulated in *KD/KO* retinas in both control and light stress conditions. We further validated our RNA results at the protein level by analysing the levels of RPE65 (a wellknown IRD gene) in the retinal pigment epithelium (RPE) of *WT/WT* and *KD/KO* retinal slices (Fig. 1B), and other proteins encoded by DE genes, such as CRYAA and CRYBB2, which encode crystallin proteins (Supplementary Figure 2). In agreement with the RNA-Seq data, the quantification of the fluorescent signal of RPE65 –as well as those of the tested CRY– were diminished in *KD/KO* RPE (Fig. 1C). In summary, our results unveil a clear pattern of DE genes between *WT/WT* and *KD/KO* retinas, most of them being downexpressed in *KD/KO* mice. The low expression level of relevant photoreceptor and RPE genes confirms the retinal dysfunction in the *KD/KO* retinas.

3.2. Antioxidant responses, mitochondrial function and glutathione metabolism are impaired in KD/KO retinas

As CERKL is involved in the oxidative stress response, we evaluated whether different antioxidant response pathways were altered in the *KD/KO* retinas. The RNA-Seq cluster analysis identified a group of DE genes related to different oxidative defence mechanisms (Fig. 2A). Antioxidant genes, such as *Sod3*, showed a decreased expression in *KD/KO* retinas, which could generate an increase in ROS, particularly after oxidative challenge. We thus assessed the antioxidant state of *KD/KO* retinas by performing retinal explants and exposing them to 500 μM sodium arsenite ($NaAsO_2$) to induce oxidative stress. H_2O_2 levels were subsequently evaluated through the ROS-Glo H_2O_2 Assay (procedure represented in Fig. 2B), yielding significantly increased levels of H_2O_2 in *KD/KO* retinas as a consequence of oxidative stress treatment (Fig. 2C).

Maintaining retinal ROS balance requires a refined equilibrium between the endogenous –due to the high metabolic rate of the retina– and exogenous –mainly light and pollution– stress factors and the enzymatic/non-enzymatic mechanisms involved in the antioxidant defence. Photoreceptor energy-demanding metabolism is principally sustained by oxidative phosphorylation (OXPHOS). In fact, mitochondria are one of the principal hubs in sensing stress and initiating antioxidant response inside cells [32]. Previous work determined that many genes encoding proteins involved in mitochondrial dynamics and metabolism were altered in *KD/KO* retinas [15], but a complete metabolic analysis was not performed. Using reverse phase protein microarrays (RPPM), we assessed the levels of more than 40 proteins involved in different metabolic pathways in *KD/KO* versus *WT/WT* retinas after light-stress insult (Supplementary Figure 3). Focusing on OXPHOS proteins, we detected a decrease in the levels of the ATP synthase subunits alpha (αF1) and beta (BF1) levels in *KD/KO* retinas, particularly after light-stress insult, whereas no differences in the levels of subunit gamma (γF1) were detected (Fig. 2D). All these alterations confirmed mitochondrial dysfunction in *KD/KO* retinas. Peroxiredoxins (PRXs) are a family of antioxidant enzymes composed of six isoforms (PRX1-6) that are expressed in the retina distributed among the different layers, cell types and organelles. For instance, PRX3 localizes to mitochondria and PRX6 is expressed in astrocytes and Müller cells [33]. Quantification of PRX3 and PRX6 protein levels through RPPM showed a trend to decrease in *KD/KO* retinas upon light-induced stress (Fig. 2E).

Remarkably, most of the DE genes included in this RNA-Seq cluster of antioxidant defence (Fig. 2A) were related to glutathione (GSH) metabolism, such as *Chac1* and *Gsto1* (upregulated in *KD/KO* versus *WT/WT*), and *Gpx3*, *Gpx8*, and *Ggt1* (downregulated in *KD/KO* versus *WT/WT*). The GSH-centered antioxidant system is one of the principal oxidative defence mechanisms of the retina by contributing to the maintenance and regulation of redox homeostasis (GSH synthesis is indicated in Fig. 3A). A decrease in GSH levels, as well as an imbalance in the ratio between the reduced (GSH) and oxidized (GSSG) forms, is associated to several retinal disorders, such as Retinitis Pigmentosa and age-related macular degeneration [6]. Taking this into consideration, we determined the levels of GSH and GSSG along with glutathione precursors levels. Our results showed a significant decrease of GSH levels as well as a significant increase in the levels of GSSG in *KD/KO* retinas compared to *WT/WT*, resulting in decreased GSH/GSSG ratio and a diminished amount of glutathione (GSH + GSSG) (Fig. 3B–E). Regarding the response to light-induced stress, GSH levels were significantly decreased in both *WT/WT* and *KD/KO* retinas, while levels of GSSG remained similar in *WT/WT* after stress (Fig. 3B–C). Therefore, GSH/GSSG ratio was significantly decreased in light-stressed *WT/WT* retinas, whereas it was not different in *KD/KO* after light stress, probably because it was already reduced in control conditions (Fig. 3D). In contrast, the total amount of glutathione (GSH + GSSG) was significantly decreased in both *WT/WT* and *KD/KO* retinas as a consequence of light-induced stress (Fig. 3E). Besides, in response to stress the levels of some GSH precursors: homocysteine and γ-glutamylcysteine levels decrease in both *WT/WT* and *KD/KO*, retinas (Fig. 3F–G). No significant differences between experimental conditions were found in the rest of the precursors (Supplementary Figure 3).

GSH/GSSG redox cycle was further studied by quantifying the levels of GSR and GPX4, enzymes directly involved in the reduction and oxidation of glutathione, through Western-blot analysis of *WT/WT* and *KD/KO* retinal lysates after light-induced stress. These results revealed *KD/KO* retinas displayed significantly higher levels of both GSR and GPX4 in response to light stress (Fig. 3H–J).

To summarize, our findings unveil the impairment of different antioxidant responses in *KD/KO* retinas. In particular, ROS detoxification, glutathione synthesis and redox cycle are already altered in *KD/KO* in basal conditions, and further oxidative challenge increases this imbalance.

3.3. KD/KO retinas and RGCs display an exacerbated PABP-mediated response

One of the few stress-related genes that showed increased expression in *KD/KO* retinas is *Pabpc4* (Fig. 2A). PABP is a main component of stress granules, membraneless organelles that are rapidly formed upon cellular stress to recruit untranslated mRNAs together with other proteins and

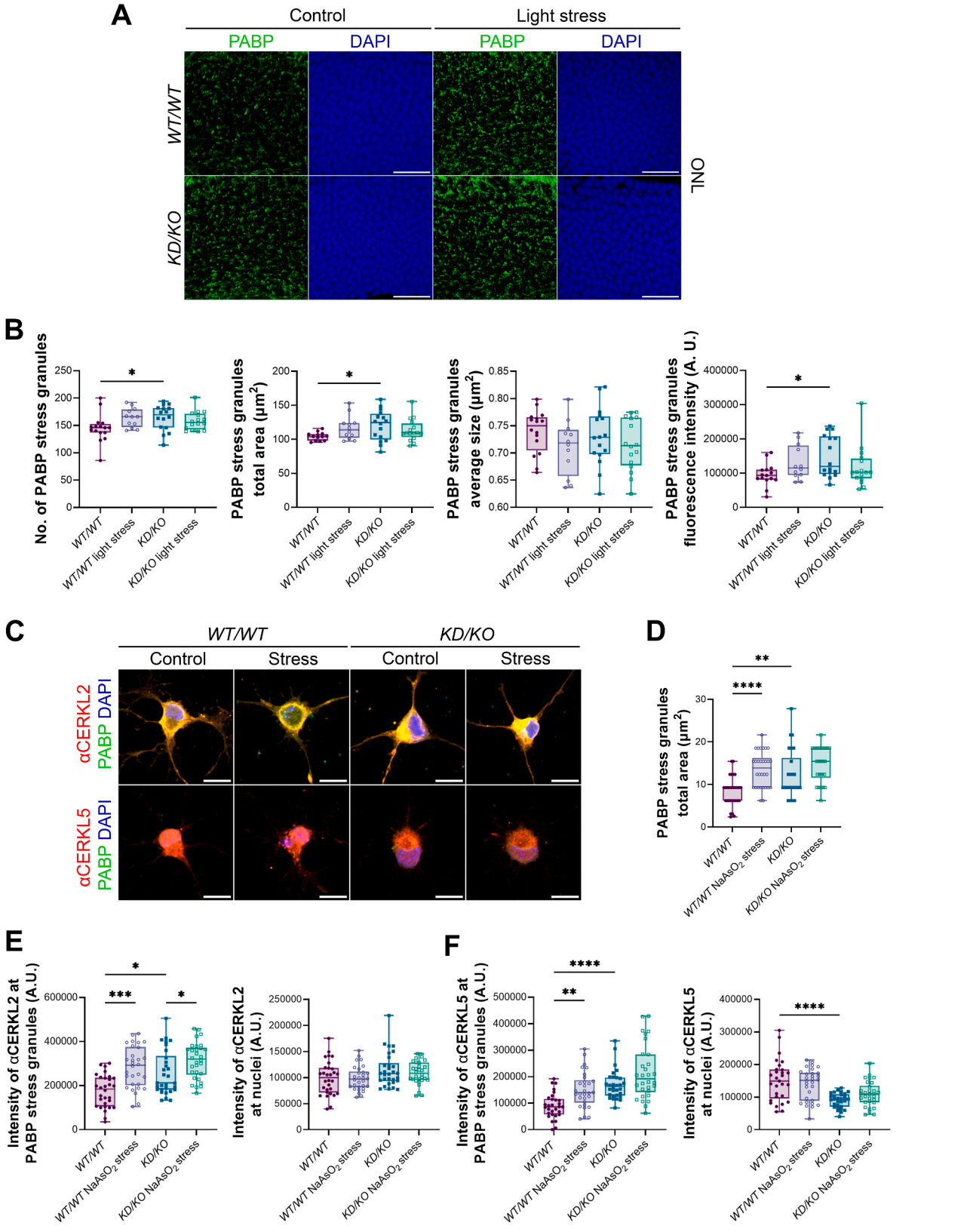

(caption on next page)

Fig. 4. PABP-mediated antioxidant response is exacerbated in *KD/KO* retinas and retinal ganglion cells (RGCs). (**A**) Representative confocal image of PABP mRNA-stress granules in the outer nuclear layer (ONL) of *WT/WT* and *KD/KO* retinas in control and light-stress conditions. Scale bar: 20 μm. (**B**) *KD/KO* retinas present higher number of PABP granules with increased levels of PABP. Quantification of the number of granules, total area, average size and PABP intensity in mRNA-stress granules. n = 12 ROIs from 4 animals per genotype and condition. (**C**) Representative confocal images of RGC somas for each studied condition. Scale bar: 10 μm. (**D**) PABP stress granules area is significantly increased in *WT/WT* RGCs upon sodium arsenite ($NaAsO_2$) induced stress as well as in *KD/KO* RGCs at basal conditions. Quantification of PABP stress granules total area in RGCs somas. n = 30 neurons from 3 animals per genotype and condition. (**E**) CERKL isoforms containing exon 2 (αCERKL2) display higher colocalization at stress granules under stress conditions, as well as in *KD/KO* RGCs in basal conditions. Quantification of CERKL isoforms displaying exon 2 colocalization at stress granules and nuclei in *WT/WT* and *KD/KO* RGCs in control and stress conditions. n = 30 neurons from 3 animals per genotype and condition. (**F**) CERKL isoforms that present exon 5 (αCERKL5) show higher colocalization at stress granules in *KD/KO* RGCs, and in *WT/WT* RGCs upon oxidative stress, as well as a significant decrease in the nuclear shift in *KD/KO* RGCs. Quantification of the intensity of CERKL isoforms expressing exon 5 at stress granules and nuclei of *WT/WT* and *KD/KO* RGCs in both control situation and under oxidative stress treatment. n = 30 neurons from 3 animals per genotype and condition. * *p-value* ≤ 0.05, ** *p-value* ≤ 0.01, *** *p-value* ≤ 0.005, **** *p-value* ≤ 0.001 (Complete images in Supplementary Fig. 5).

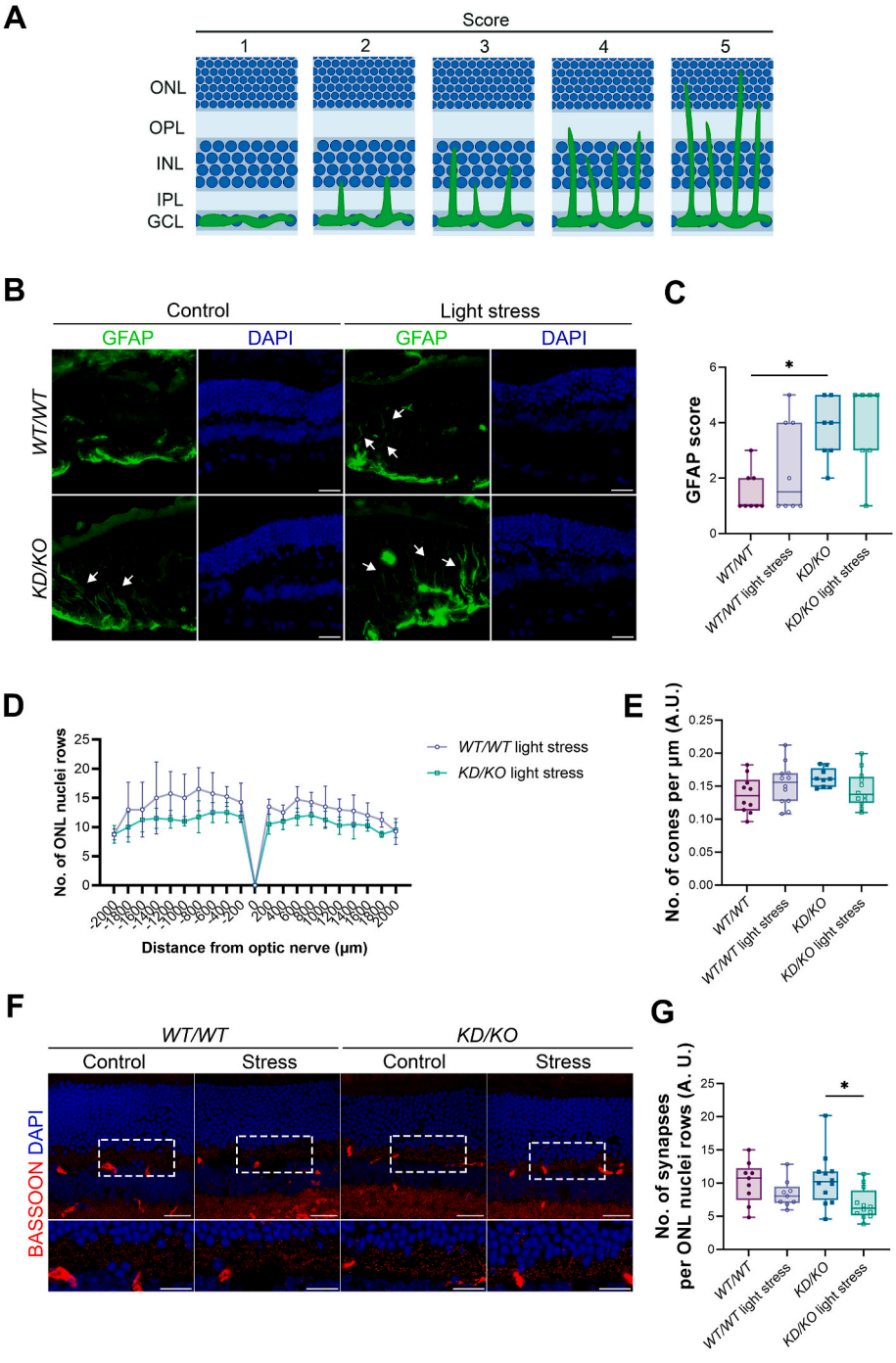

Fig. 5. Retinal remodelling two weeks after light-stress injury in *KD/KO* retinas. (**A**) Schematic representation of GFAP scores based on [34]. Reactive astrocytes and Müller glial cells are represented in green. ONL: outer nuclear layer, OPL: outer plexiform layer, INL: inner nuclear layer, IPL: inner plexiform layer, GCL: ganglion cell layer. (**B**) Glial branching reaches higher retinal layers in *KD/KO*. Representative fluorescence microscopy images of GFAP-positive astrocytes (green) and nuclei staining (DAPI in blue) in *WT/WT* and *KD/KO* retinas 2 weeks after light-stress treatment. White arrows indicate GFAP-positive ramifications. Scale bar: 20 μm. (**C**) GFAP score quantification shows higher levels of GFAP branching in *KD/KO* retinas. n = 7–8 ROIs from 4 animals per genotype and condition. (**D**) *KD/KO* retinas show a tendency to decreased number of photoreceptor nuclei rows two weeks after light insult. Quantification of photoreceptor nuclear rows (ONL) showing *WT/WT* and *KD/KO* values after light stress treatment. (**E**) No differences in the number of cones along the retina between all conditions and genotypes were observed. (**F**) Diminished number of synapses in *KD/KO* retinas as a late consequence of light stress. Representative confocal images of *WT/WT* and *KD/KO* retinal slices after stress damage immunodetecting BASSOON (red) and staining nuclei (DAPI in blue). Scale bar: 25 μm. High magnification images exhibit photoreceptor synapse buttons minutely. Scale bar: 15 μm. (**G**) Quantification of the number of synaptic buttons labeled with BASSOON normalized by the rows of photoreceptor nuclei. n = 8 ROIs from 4 retinas per genotype and condition. * *p-value* ≤ 0.05. (Complementary data in Supplementary Fig. 6). (For interpretation of the references to colour in this figure legend, the reader is referred to the Web version of this article.)

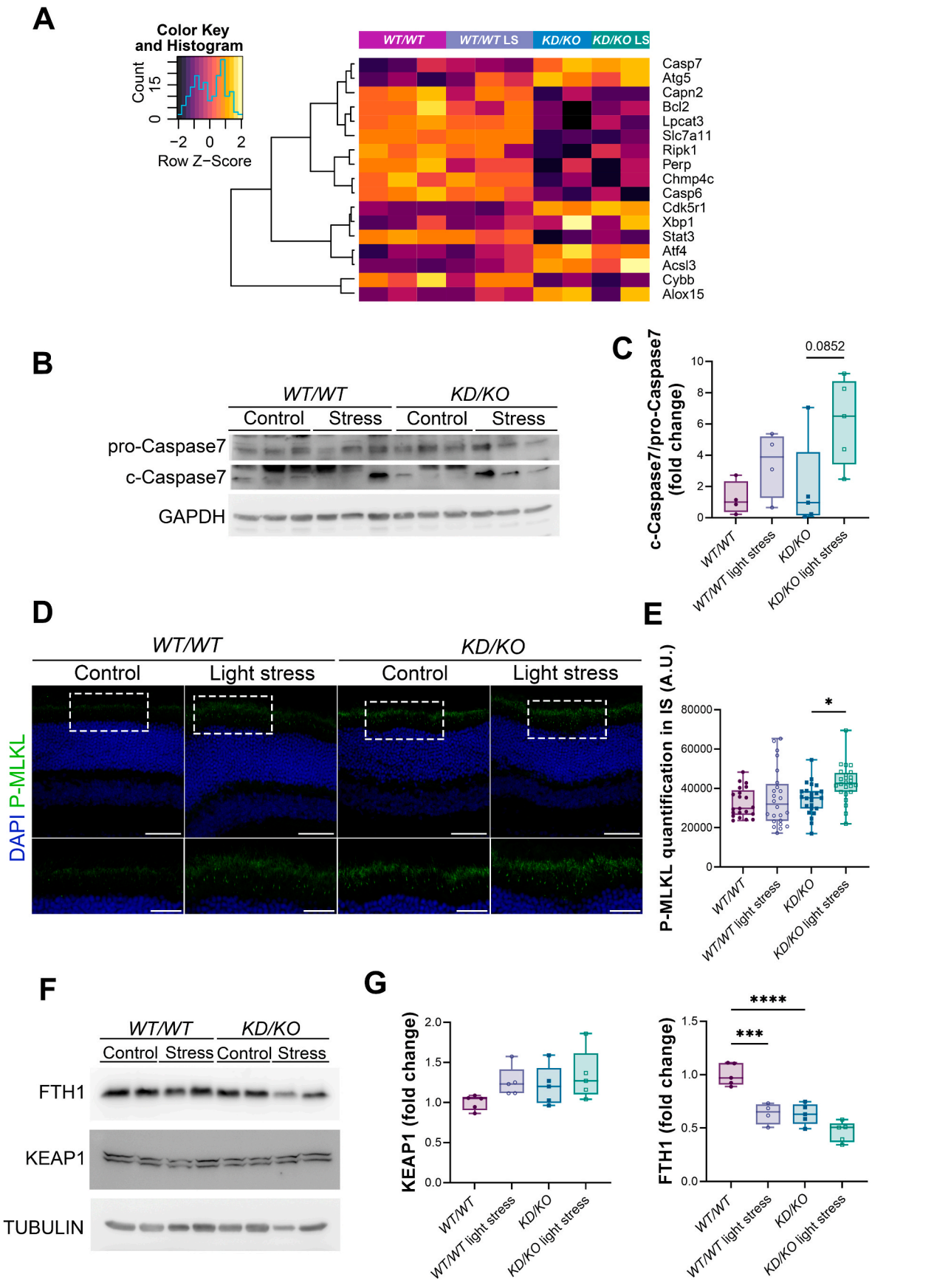

(caption on next page)

Fig. 6. Activation of different cell death mechanisms in *KD/KO* retinas upon light-stress damage. (**A**) Heatmap showing hierarchical clustering of differentially expressed genes involved in cell death pathways. (**B, C**) Activation of apoptosis in *KD/KO* retinas as a response to light stress through cleavage of CASPASE-7. (**B**) Western-blot of *WT/WT* and *KD/KO* retinal lysates immunodetecting CASPASE-7 and its cleaved isoform. GAPDH is used as loading control. (**C**) Quantification of cleaved-CASPASE-7:pro-CASPASE7 ratio (c-Caspase7/pro-Caspase7) shows a moderate increment in *KD/KO* retinas after stress treatment. (**D, E**) Necroptosis is triggered after MLKL phosphorylation in photoreceptor inner segments of *KD/KO* retinas under light-stress injury. (**D**) Representative fluorescent image of P-MLKL (green) in *WT/WT* and *KD/KO* retinas under light stress. DAPI is used to stain nuclei (blue). Scale bar: 50 μm. High magnification images show photoreceptor inner segment in more detail. Scale bar: 25 μm. (**E**) Quantification of P-MLKL fluorescence in the inner segment (IS) of WT and *KD/KO* photoreceptors after light-induced stress treatment. n = 24 ROIs from 4 animals per genotype and condition. (**F, G**) *KD/KO* retinas display decreased levels of FTH1 in both basal and light-induced stress conditions, reaching ferroptosis. (**F**) Western blot of *WT/WT* and *KD/KO* retinal homogenates after light-stress treatment immunodetecting FTH1, KEAP1 and TUBULIN (loading control). (**G**) Measurement of FTH1 and KEAP1 protein levels normalized using TUBULIN in WT and *KD/KO* retinal lysates upon light damage. n = 5 retinas per genotype and condition. * *p-value* ≤ 0.05, ** *p-value* ≤ 0.01, *** *p-value* ≤ 0.005, **** *p-value* ≤ 0.001. (For interpretation of the references to colour in this figure legend, the reader is referred to the Web version of this article.)

protect them from degradation [7]. These stress assemblies play key roles in cell thriving and survival upon stress [8]. In previous studies, CERKL has been described to interact with different proteins involved in the formation of stress granules, such as eIF3B and PABP [20]. Taking advantage of the *KD/KO* mouse model, we aimed to examine the stress granule-mediated response to light-induced stress in *KD/KO* retinas. Analysis and quantification of PABP stress granules in *WT/WT* and *KD/KO* outer nuclear layer (ONL) after light insult revealed a significant increase in the number and total area occupied by stress granules in *KD/KO* ONL in control conditions, while the average size of stress granules is the same between genotypes and conditions (Fig. 4A–B). Moreover, we found a significantly higher intensity of PABP in stress granules in *KD/KO* retinas in basal conditions (Fig. 4B).

Additionally, similar experiments were performed in *WT/WT* and *KD/KO* retinal ganglion cell (RGCs) primary cultures where oxidative stress has been induced with sodium arsenite ($NaAsO_2$). PABP and CERKL were immunodetected to study stress granules formation and colocalization with CERKL in the somas of *WT/WT* and *KD/KO* RGCs (Fig. 4C, complete images of RGCs in Supplementary Figure 4), with two in house antibodies that recognize different CERKL isoforms [21]: αCERKL2 recognizes an epitope encoded in exon 2 (Fig. 4C upper panel, Supplementary Figure 5A) whereas αCERKL5 recognizes an epitope encoded in exon 5 (Fig. 4C lower panel, Supplementary Figure 5B). A significant increase in the total area occupied by stress granules in the cytoplasm of *WT/WT* RGCs was clearly detected as a response to oxidative stress. Interestingly, we observed a similar increase in *KD/KO* RGCs at basal conditions (Fig. 4D), in agreement with the results obtained in vivo in *KD/KO* photoreceptors (Fig. 4A–B). Colocalization analysis showed higher colocalization of isoforms detected by αCERKL2 with stress granules in *KD/KO* RGCs compared with *WT/WT* in basal conditions, and a significant higher colocalization with stress granules in both *WT/WT* and *KD/KO* RGCs upon oxidative stress treatment (Fig. 4E). No changes in the localization of αCERKL2 at the nuclei were observed (Fig. 4E). On the other hand, CERKL isoforms that contain exon 5-peptide displayed a similar pattern of colocalization with stress granules compared to CERKL2 in all conditions, but for a significant decrease of nuclear αCERKL5 localization in *KD/KO* RGCs (Fig. 4F).

Therefore, PABP stress granules-mediated response is already highly activated in *KD/KO* whole retinas and in primary RGCs in basal conditions at similar levels to *WT/WT* retinas upon stress damage. Nonetheless, *KD/KO* retinas cannot further respond to additional external oxidative stress stimuli.

3.4. Retinal remodelling in KD/KO two weeks after light-induced injury

In order to study late-onset effects of light stress damage in *KD/KO* retinas, we performed light stress treatment in *WT/WT* and *KD/KO* mice and assessed their retinas two weeks after injury. Glial cells participate actively in retinal homeostasis through morphological and biochemical changes. In reactive gliosis, GFAP-positive astrocytes specifically undergo hypertrophy by projecting ramifications from the inner up to the outer layers of the retina, and Müller glial cells also start expressing GFAP [4]. To analyze the level of gliosis, we have followed a pre-set scale with different scores of glia activation depending on the retinal layers reached by glial ramifications [34], in which higher scores mean more advanced gliosis (Fig. 5A). We detected GFAP-positive reactive cells in retinal cryosections of *WT/WT* and *KD/KO* mice two weeks after light-stress treatment (Fig. 5B, white arrows). Score analysis revealed an increased gliosis in light stress conditions that does not reach significance within each genotype. However, we did find significant higher levels of gliosis in *KD/KO* versus *WT/WT* retinas at basal conditions, meaning that *Cerkl* downregulation produces a strong glial activation without further stressing factors (Fig. 5C).

Furthermore, we tested the effects of long-term light-induced damage in *KD/KO* retinas by performing comparative morphometric analyses and layer structure assessment. Outer nuclear layer (ONL), inner nuclear layer (INL) and total retinal thickness as well as the number of photoreceptor nuclei rows were measured in *WT/WT* and *KD/KO* retinas. For most measurements, no significant differences between genotype or condition were observed (Supplementary Figure 6). However, focusing on the number of photoreceptor nuclei rows after light stress, we detected a moderate decrease in the number of photoreceptor nuclear rows in *KD/KO* compared to *WT/WT* retinas (Fig. 5D). This photoreceptor slight decrease most probably corresponds to rod's death, as the number of cones per area is preserved in all genotypes and conditions (Fig. 5E). Nonetheless, when considering this discrete ONL thinning in the retinas of 6-months-old animals, we should take into account that the retinal degeneration in our *KD/KO* model progresses slowly and is detected at older ages (more than 12-months-old animals), and what we observe here in response to light stress are the initial steps leading to retinal degeneration.

We also checked whether synaptic retinal remodelling might be occurring as a late response to light stress by quantifying the number of photoreceptor synapses in post-synaptic inner neurons through immunodetection of the synapse marker BASSOON in *WT/WT* and *KD/KO* retinas (Fig. 5F). Quantification of synapses in the outer plexiform layer suggested *KD/KO* retinas presented a significant decrease in the number of synapses per photoreceptor as a late consequence of light-induced stress (Fig. 5G).

In summary, retinal remodelling is observed in *KD/KO* mice two weeks after light-stress treatment via both moderate photoreceptor loss and a decrease in the number of synapses per photoreceptor.

3.5. Cell death mechanisms activation after light stress treatment in KD/KO retinas

As an ultimate outcome of defective antioxidant responses to oxidative damage, apoptotic and non-apoptotic programmed cell death pathways are eventually triggered, being the main cause of retinal neurodegeneration and vision loss in patients of retinal dystrophies [35,36]. Therefore, we checked the regulation of different degenerative mechanisms performing a cluster analysis of RNA-Seq results, which resulted in a group of DE genes associated with various cell death pathways (Fig. 6A). Among them, we found DE genes related to apoptosis (e.g., *Casp7*, *Bcl2* and *Casp6*), necroptosis (e.g., *Ripk1*) and ferroptosis (e.g., *Slc7a11* and *Alox15*).

Among the different programmed cell death mechanisms, apoptosis has been considered the main cell death pathway occurring in the retina [35]. In the apoptotic process, both intrinsic and extrinsic apoptotic signalling cascades ultimately activate caspase-3 and caspase-7 as final effectors. We checked out the activation of apoptosis by quantifying the levels of cleaved CASPASE-7 (c-Caspase7) in comparison to uncleaved CASPASE-7 levels (pro-Caspase7) through Western-blot analysis of *WT/WT* and *KD/KO* retinal lysates upon light-induced injury (Fig. 6B). These results revealed a moderate but non-significant increase in the cleavage of pro-apoptotic CASPASE-7 in *KD/KO* retinas after stress treatment (Fig. 6C).

Moreover, other regulated degenerative mechanisms can be triggered in the retina, such as necroptosis and ferroptosis. In the necroptotic pathway, different kinases (RIPK1 and RIPK3) are activated in cascade to finally phosphorylate MLKL. Phosphorylated MLKL (P-MLKL) is then transported to the cell membrane, where it causes cell death by disruption of membrane integrity [37,38]. Thus, we assessed the location and quantity of P-MLKL in the photoreceptor membrane of *WT/WT* and *KD/KO* retinas after light-stress insult (Fig. 6D). In light-stressed *KD/KO* retinas the levels of P-MLKL localizing to the photoreceptor membrane were significantly increased in comparison to control *KD/KO*, indicating that necroptosis is triggered in *KD/KO* photoreceptors as a consequence of light-stress injury (Fig. 6E).

Ferroptosis is a programmed cell death pathway characterized by iron accumulation, oxidative stress, loss of mitochondrial integrity and low glutathione levels, which results in oxidation of nucleic acids, proteins, and lipids. All these ROS-derived alterations finally rise lethal calcium influx [39]. The iron responsive genes, such as FTH1 and other proteins involved in the ferroptotic cascade are induced by binding of NRF2 to the antioxidant responsive elements (AREs) in their promoters [40]. NRF2 is a master antioxidant transcription factor regulator whose levels are tightly controlled by the ubiquitin ligase KEAP1, which ubiquitylates NRF2, tagging it for proteasome degradation [41]. Notably, the NRF2/KEAP1 axis is slightly impaired in *KD/KO* retinas in basal conditions, as the transcriptional levels of *Nfe2l2* (the gene encoding NRF2) are slightly but significantly reduced down to 80% in *KD/KO* retinas compared to *WT/WT,* whereas those of KEAP1 are increased around 1.3-fold (RNA-Seq Supplementary Data). Therefore, we assessed the levels of KEAP1 and FTH1 (a ferroptosis suppressor gene induced by NRF2) by Western-blot analysis of *WT/WT* and *KD/KO* retinal lysates after light stress (Fig. 6F). In agreement with the RNA-Seq data, quantification of the ubiquitin ligase KEAP1 levels revealed a slight increase in *WT/WT* retinas in response to stress, as well as in *KD/KO* retinas in control and stress conditions. As a consequence, the levels of FTH1 were significantly reduced in light-stressed *WT/WT* and control *KD/KO* retinas, compared to control *WT/WT*. In addition, *KD/KO* retinas showed further decrease in the levels of FTH1 upon light-induced stress (Fig. 6G). The final consequence of the observed alterations is the activation of ferroptosis.

To conclude, multiple mediated cell death mechanisms are activated at different levels in *KD/KO* retinas in response to light-induced stress.

4. Discussion

Inherited retinal dystrophies (IRDs) are a heterogeneous group of disorders caused by mutations in more than 300 genes/loci (RetNet, the Retinal Information Network, 1996–2023, https://web.sph.uth.edu/RetNet/). IRD-causative genes display many different functions in photoreceptor and other retinal cells, from specific structural roles (e.g., *CEP290, PROM1*), photoreception and phototransduction (e.g., *Rhodopsin, PDE6B*) or photoreceptor differentiation (e.g., *NRL*, *NR2E3*). Although the specific biochemical function is not always precisely determined (as is the case for *EYS, FAM161A or RPGR,* among others), the mutations in IRD genes cause the same phenotypic outcome: degeneration of photoreceptor cells and progressive visual decline, which eventually leads to blindness. Some IRDs are caused by failure in specific enzymatic and non-enzymatic protective antioxidant systems, thus inducing a higher susceptibility to oxidative stress caused by endogenous and/or exogenous damaging factors, such as the continuous impact of light [42,43]. In this context, *CERKL* has been described as a resilience gene against oxidative stress in the retina and other tissues, although its particular and specific function has not yet been fully elucidated. With this work, we aimed to deepen in the CERKL protective role in the retina, particularly in response to acute light stress treatment, first by identifying differentially expressed genes upon light stress robustly associated to *Cerkl* knockdown; and second, by assessing antioxidant mechanisms in the retinas in the $Cerkl^{KD/KO}$ *(KDKO)* model in order to identify potential actionable pathways for specific antioxidant therapeutic treatments.

Notably, results from RNA-Seq showed consistent transcriptional differences between genotypes, but very slight variations in response to light stress. Although surprising at first sight, we should note that transcriptomic analysis was performed after 1 h of light stress, and most probably, early oxidative defence pathways or even cell death mechanisms (see below) activation after acute injury rely on post-transcriptional but not transcriptional events. Longer exposure to light might reveal further altered cell pathways, although chronic light stress most probably induces strong retinal remodelling and inflammation as reported in Ref. [22]. Overall, our results though reinforce that knockdown of *Cerkl* alters directly or indirectly the expression of multiple genes, being most of them downregulated, including many IRD and phototransduction/visual cycle genes, thus reflecting photoreceptor and RPE dysfunction.

Previous studies reported that wild type CERKL was shown to be involved in the formation of RNA stress granules and P-bodies [20]. Here we report for the first time that mRNA stress granule response is exacerbated in *KD/KO* retinas in basal conditions, reaching levels similar to those of stressed *WT/WT* retinas. Surprisingly, acute light/-oxidative treatment did not cause an increase of stress granule response in *KD/KO* retinal cells, compared to the already overactivated response in basal conditions. On the other hand, a similar response was detected when assessing the GSH/GSGG ratio and the total quantity of glutathione in *WT/WT* vs *KD/KO* retinas. Again, in the absence of further environmental stressors, glutathione metabolism was already impaired in *KD/KO* retinas, showing similar levels of GSH/GSSG balance and glutathione total amount as *WT/WT* light-exposed retinas.

Among all the enzymatic oxidative defence mechanisms, CERKL has been shown to interact with the antioxidant enzyme TRX2 to ensure its redox function [17]. In this work we have also found alterations in the levels of other antioxidant enzymes in *KD/KO* retinas, such as PRX3 and PRX5, particularly after light-induced stress. Concerning the enzymatic machinery involved in glutathione metabolism, our findings showed increased levels of different enzymes, such as GSR, GPX4 and CHAC1, in *KD/KO* light-exposed retinas. Overregulation of these proteins, particularly GPX4 and CHAC1, is indicative of oxidative stress protection [44–46], whereas GPX downregulation is related to increased oxidative damage, as shown in *rd1* mouse model retinas [47]. Thus, in *KD/KO* retinas, downregulation of PRXs and overregulation of glutathione related enzymes might also occur as a compensatory reaction to the lowered levels of GSH to assure the glutathione-based response to light stress.

All these findings, together with those related to stress granule formation and the alterations detected in NRF2/KEAP1 axis, indicate that *KD/KO* retinas already suffer from endogenous oxidative stress in normal conditions and fail to further activate antioxidant mechanisms against external stress stimuli.

The contribution of CERKL to mitochondrial dynamics and metabolism has already been assessed in previous work, in which *CERKL/Cerkl* downregulation resulted in smaller and dysfunctional mitochondria, whereas *CERKL* overexpression protected mitochondrial morphology and function from oxidative stress [15,18,19]. Here, we also describe alterations in the levels of different subunits of the ATP

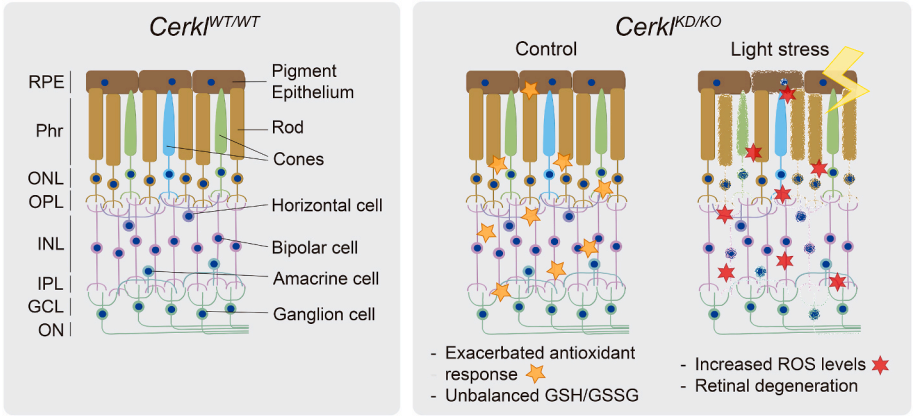

Fig. 7. Model of retinal degeneration in *Cerkl*$^{KD/KO}$ due to oxidative stress response dysregulation. The *WT/WT* retina shows the laminar distribution of retinal neuronal cells (right panel). In contrast, *KD/KO* retinas show: i) an upregulation of oxidative stress response (e.g., stress granule formation and gliosis) and ii) unbalanced glutathione metabolites, even in basal conditions. This dysregulated response is further exacerbated upon light-stress, with increased H_2O_2 → ROS production, which eventually leads to retinal degeneration. RPE: retinal pigment epithelium, Phr: photoreceptor layer, ONL: outer nuclear layer, OPL: outer plexiform layer, INL: inner nuclear layer, IPL: inner plexiform layer, GCL: ganglion cell layer, ON: optic nerve.

synthase upon *Cerkl* knockdown. As a vicious circle, energy-supply mechanisms produce ROS, but ROS can also damage energy-supply systems. On the other hand, if there is not sufficient energy production the repair systems cannot act properly, and the resulting imbalance eventually may lead to cell death [48]. Given that, apart from alterations in mitochondrial metabolism, we also describe increased levels of H_2O_2 and ROS and dysregulated antioxidant responses in *KD/KO* light-exposed retinas, it is difficult to elucidate which is the first link in the chain initiating this vicious circle.

CERKL is a gene with highly complex regulation, including different transcription start sites and alternative splicing events. As a result, at least four main protein isoforms can be found in the human, and three in the mouse retinas [49]. These isoforms display different protein domains and might thus play different roles. Interestingly, although *Cerkl* expression is not increased after light stress in the wild-type retinas, the subcellular localization of different CERKL protein isoforms shifts, thus reflecting post-translational regulation in response to stress. Thus, while CERKL isoforms containing either exon 2 and/or exon 5 are localized ubiquitously through the soma and dendrites of *WT/WT* RGCs, in *KD/KO* RGCs, a limited pool of exon 2-containing isoforms is detected in the nuclei, but most of the residual CERKL mainly localizes to stress granules, as a crucial CERKL-mediated stress response mechanism.

As a common point in different neurodegenerative retinal disorders, glial cells are activated in response to damage and degeneration of retinal cells, eventually inducing an inflammation state in the retina [50]. Accordingly, our results showed an increment of gliosis in *KD/KO* retinas, regardless of light-stress treatment, that is indicative of chronic damage in *KD/KO* retinas, and results in deleterious effects that may contribute to retinal neurodegeneration [4]. Moreover, we observed a late light-responsive loss of synaptic contacts between photoreceptor cells and post-synaptic neurons in the *KD/KO* retinas (at two weeks post-injury), suggesting retinal connection remodelling as part of the neurodegenerative process as reviewed in Refs. [51,52].

As a final outcome of light-induced stress, impaired antioxidant responses and gliosis, we observed activation of several cell death mechanisms at different levels, including necroptosis, ferroptosis and apoptosis. Activation of necroptosis in *KD/KO* photoreceptors promotes cell death, as an expected response to light-stress damage [53]. Moreover, the detected increase in ferroptosis in *KD/KO* retinas may be due to several alterations: i) significantly lower RNA levels of the antioxidant response master regulator NRF2 (log_2 Fold Change of −0.3383), ii) the slight increase in KEAP1 protein levels, the ubiquitin ligase that promotes NRF2 degradation [41]), and iii) the subsequent significant decrease of FTH1, an anti-ferroptotic protein involved in ferrous iron scavenging [54,55], as a consequence of the alteration of the glutathione system [44,46], leading to iron release. Finally, and in agreement with other IRD mouse models, apoptosis –although detectable– was not the principal cell death mechanism activated in *KD/KO* retinas [56]. Coherently, the inflammatory response mediated by glia is strongly associated with non-apoptotic cell death pathways, such as ferroptosis and necroptosis. Overall, *KD/KO* light-exposed retinas display several cell death mechanisms, which might be cell-specific. Further work is required to assess the relevance of each pathway in retinal degeneration.

5. Conclusions

Altogether, these studies provide further evidence of the importance of CERKL for the proper regulation, control, and balance of antioxidant systems in response to acute light stress in the retina. In addition, *Cerkl* downregulation causes retinal oxidative stress in basal conditions, and this chronic overactivation of different oxidative defence mechanisms does not allow to respond further upon stress injury. Eventually, the balance between antioxidant mechanisms and ROS levels is altered and triggers different cell death mechanisms in *KD/KO* retinas. Our findings (model in Fig. 7) shed light on the pathogenesis mechanisms of *CERKL* mutations, which eventually cause retinal degeneration and blindness by impairing the oxidative stress response in the retina. In this context, specific therapeutical approaches by gene therapy adding *CERKL* or by antioxidant treatments targeting key actionable pathways [57] seem promising strategies to halt IRD disease progression.

Author contributions

Conceptualization and supervision, G.M. and S.M.; methodology, R. G.-A., E.B.D., M.A.A. and C.N.A.; bioinformatical analysis, C.H.-U.; formal analysis, R.G.-A., E.B.D., C.H.-U., M.A.A., C.N.A., J.M.C., J.G.-F., F.V.P., G.M. and S.M.; resources, J.M.C., F.V.P., G.M. and S.M.; writing-original draft preparation, R.G.-A., G.M. and S.M.; writing-review and editing, R.G.-A., G.M. and S.M. All authors have revised and agreed to the final draft of the manuscript.

Funding

S.M. had a postdoctoral contract with CIBERER/ISCIII, R.G.-A. is recipient of the FI-DGR grant (Generalitat de Catalunya). This research was supported by grants ACCI 2019 (CIBERER/ISCIII) to S.M. and ACCI 2021 (CIBERER/ISCIII) to S.M. and J.M.C.; PID2019-108674RB-100 to J.M.C. (Ministerio de Ciencia e Innovación/FEDER), PID2020-117820 GB-I00 (Ministerio de Ciencia e Innovación/FEDER) to J.G.-F., 2021SGR-01093 (Generalitat de Catalunya), PID2019-108578RB-I00 to G.M and S.M. and PID2022-140957OB-I00 to G.M (both financed by Ministerio de Ciencia e Innovación/FEDER).

Declaration of competing interest

None of the authors of the manuscript by García-Arroyo et al.

"**Exacerbated response to oxidative stress in the Retinitis Pigmentosa *Cerkl*$^{KD/KO}$ mouse model induces retinal degeneration upon acute light injury**" has any conflict of interest to declare.

Data availability

Data will be made available on request.

Acknowledgments

We acknowledge Dr. Rafael Artuch and Dr. José F. Abril for their insightful comments, as well as past and present members of our research group for helpful discussions. We are also grateful to the associations of patients affected by retinal dystrophies for their constant support.

Appendix A. Supplementary data

Supplementary data to this article can be found online at https://doi.org/10.1016/j.redox.2023.102862.

References

[1] V.E. Baksheeva, V.V. Tiulina, N.K. Tikhomirova, O.S. Gancharova, S.V. Komarov, P.P. Philippov, A.A. Zamyatnin, I.I. Senin, E.Y. Zernii, Suppression of light-induced oxidative stress in the retina by mitochondria-targeted antioxidant, Antioxidants 8 (2019), https://doi.org/10.3390/antiox8010003.

[2] E.B. Domènech, G. Marfany, The relevance of oxidative stress in the pathogenesis and therapy of retinal dystrophies, Antioxidants 9 (2020) 1–22, https://doi.org/10.3390/antiox9040347.

[3] K. Rashid, I. Akhtar-Schaefer, T. Langmann, Microglia in retinal degeneration, Front. Immunol. 10 (2019) 1–19, https://doi.org/10.3389/fimmu.2019.01975.

[4] P.V. Subirada, M.C. Paz, M.E. Ridano, V.E. Lorenc, M.V. Vaglienti, P.F. Barcelona, J.D. Luna, M.C. Sánchez, A journey into the retina: Müller glia commanding survival and death, Eur. J. Neurosci. 47 (2018) 1429–1443, https://doi.org/10.1111/ejn.13965.

[5] S. Mirra, G. Marfany, Mitochondrial gymnastics in retinal cells: a resilience mechanism against oxidative stress and neurodegeneration, in: Adv Exp Med Biol, 2019, pp. 513–517, https://doi.org/10.1007/978-3-030-27378-1_84.

[6] P.G. Sreekumar, D.A. Ferrington, R. Kannan, Glutathione metabolism and the novel role of mitochondrial gsh in retinal degeneration, Antioxidants 10 (2021) 1–18, https://doi.org/10.3390/antiox10050661.

[7] P. Anderson, N. Kedersha, Stress granules, Curr. Biol. 19 (2009) 397–398, https://doi.org/10.1016/j.cub.2009.03.013.

[8] W. van Leeuwen, C. Rabouille, Cellular stress leads to the formation of membraneless stress assemblies in eukaryotic cells, Traffic 20 (2019) 623–638, https://doi.org/10.1111/tra.12669.

[9] T.S. Aleman, N. Soumittra, A.V. Cideciyan, A.M. Sumaroka, V.L. Ramprasad, W. Herrera, E.A.M. Windsor, S.B. Schwartz, R.C. Russell, A.J. Roman, C. F. Inglehearn, G. Kumaramanickavel, E.M. Stone, G.A. Fishman, S.G. Jacobson, CERKL mutations cause an autosomal recessive cone-rod dystrophy with inner retinopathy, Invest. Ophthalmol. Vis. Sci. 50 (2009) 5944–5954, https://doi.org/10.1167/iovs.09-3982.

[10] M. Tuson, G. Marfany, R. Gonzàlez-Duarte, Mutation of CERKL, a novel human ceramide kinase gene, causes autosomal recessive retinitis pigmentosa (RP26), Am. J. Hum. Genet. 74 (2004) 128–138.

[11] A.O. Khan, L. Abu-Safieh, Rod-Cone dystrophy with initially preserved visual acuity despite early macular involvement suggests recessive CERKL mutations, Ophthalmic Genet. 36 (2015) 369–372, https://doi.org/10.3109/13816810.2014.889168.

[12] M. Ali, V.L. Ramprasad, N. Soumittra, M.D. Mohamed, H. Jafri, M. Danciger, M. Mckibbin, G. Kumaramanickavel, C.F. Inglehearn, A missense mutation in the nuclear localization signal sequence of CERKL (p .R106S) causes autosomal recessive retinal degeneration, Mol. Vis. 14 (2008) 1960–1964.

[13] X. Hu, Z. Lu, S. Yu, J. Reilly, F. Liu, D. Jia, Y. Qin, S. Han, X. Liu, Z. Qu, Y. Lv, J. Li, Y. Huang, T. Jiang, H. Jia, Q. Wang, J. Liu, X. Shu, Z. Tang, M. Liu, CERKL regulates autophagy via the NAD-dependent deacetylase SIRT1, Autophagy 15 (2019) 453–465, https://doi.org/10.1080/15548627.2018.1520548.

[14] S. Huang, Z. Hong, L. Zhang, J. Guo, Y. Li, K. Li, CERKL alleviates ischemia reperfusion-induced nervous system injury through modulating the SIRT1/PINK1/Parkin pathway and mitophagy induction, Biol. Chem. 403 (2022) 1–11.

[15] S. Mirra, R. García-Arroyo, E.B. Domènech, A. Gavaldà-Navarro, C. Herrera-Úbeda, C. Oliva, J. Garcia-Fernàndez, R. Artuch, F. Villarroya, G. Marfany, CERKL, a retinal dystrophy gene, regulates mitochondrial function and dynamics in the mammalian retina, Neurobiol. Dis. 156 (2021), 105405, https://doi.org/10.1016/j.nbd.2021.105405.

[16] M. Tuson, A. Garanto, R. Gonzàlez-Duarte, G. Marfany, Overexpression of CERKL, a gene responsible for retinitis pigmentosa in humans, protects cells from apoptosis induced by oxidative stress, Mol. Vis. 15 (2009) 168–180.

[17] C. Li, L. Wang, J. Zhang, M. Huang, F. Wong, X. Liu, F. Liu, X. Cui, G. Yang, J. Chen, Y. Liu, J. Wang, S. Liao, M. Gao, X. Hu, X. Shu, Q. Wang, Z. Yin, Z. Tang, M. Liu, CERKL interacts with mitochondrial TRX2 and protects retinal cells from oxidative stress-induced apoptosis, Biochim. Biophys. Acta, Mol. Basis Dis. 1842 (2014) 1121–1129, https://doi.org/10.1016/j.bbadis.2014.04.009.

[18] R. García-Arroyo, A. Gavaldà, F. Villarroya, G. Marfany, S. Mirra, Overexpression of CERKL protects retinal pigment epithelium mitochondria from oxidative stress effects, Antioxidants 10 (2021) 1–16.

[19] R. García-Arroyo, G. Marfany, S. Mirra, CERKL, a retinal dystrophy gene, regulates mitochondrial transport and dynamics in hippocampal neurons, Int. J. Mol. Sci. 23 (2022), https://doi.org/10.3390/ijms231911593.

[20] A. Fathinajafabadi, E. Pérez-Jiménez, M. Riera, E. Knecht, R. Gonzàlez-Duarte, CERKL, a retinal disease gene, encodes an mRNA-binding protein that localizes in compact and untranslated mRNPs associated with microtubules, PLoS One 9 (2014), https://doi.org/10.1371/journal.pone.0087898.

[21] E.B. Domènech, R. Andres, M.J. López-Iniesta, S. Mirra, R. García-Arroyo, S. Milla, F. Sava, J. Andilla, P.L. Alvarez, P. De La Villa, R. Gonzàlez-Duarte, G. Marfany, A new Cerkl mouse model generated by CRISPR-cas9 shows progressive retinal degeneration and altered morphological and electrophysiological phenotype, Invest. Ophthalmol. Vis. Sci. 61 (2020), https://doi.org/10.1167/IOVS.61.8.14.

[22] O. Kutsyr, X. Sánchez-Sáez, N. Martínez-Gil, E. de Juan, P. Lax, V. Maneu, N. Cuenca, Gradual increase in environmental light intensity induces oxidative stress and inflammation and accelerates retinal neurodegeneration, Invest. Ophthalmol. Vis. Sci. 61 (2020), https://doi.org/10.1167/IOVS.61.10.1.

[23] M. Samardzija, V. Todorova, L. Gougoulakis, M. Barben, S. Nötzli, K. Klee, F. Storti, A. Gubler, C. Imsand, C. Grimm, Light stress affects cones and horizontal cells via rhodopsin-mediated mechanisms, Exp. Eye Res. 186 (2019), 107719, https://doi.org/10.1016/j.exer.2019.107719.

[24] M.V. Kuleshov, M.R. Jones, A.D. Rouillard, N.F. Fernandez, Q. Duan, Z. Wang, S. Koplev, S.L. Jenkins, K.M. Jagodnik, A. Lachmann, M.G. McDermott, C. D. Monteiro, G.W. Gundersen, A. Maayan, Enrichr: a comprehensive gene set enrichment analysis web server 2016 update, Nucleic Acids Res. 44 (2016), https://doi.org/10.1093/nar/gkw377. W90–W97.

[25] Z. Xie, A. Bailey, M.V. Kuleshov, D.J.B. Clarke, J.E. Evangelista, S.L. Jenkins, A. Lachmann, M.L. Wojciechowicz, E. Kropiwnicki, K.M. Jagodnik, M. Jeon, A. Ma'ayan, Gene set knowledge discovery with Enrichr, Curr Protoc 1 (2021), https://doi.org/10.1002/cpz1.90.

[26] E.Y. Chen, C.M. Tan, Y. Kou, Q. Duan, Z. Wnag, G.V. Meirelles, N.R. Clark, A. Ma'ayan, Enrichr: interactive and collaborative HTML5 gene list enrichment analysis tool Edward, BCM Bioinf. 14 (2013) 1–15, https://doi.org/10.1007/s00701-014-2321-4.

[27] S.X. Ge, E.W. Son, R. Yao, iDEP: an integrated web application for differential expression and pathway analysis of RNA-Seq data, BMC Bioinf. 19 (2018) 1–24, https://doi.org/10.1186/s12859-018-2486-6.

[28] J. Escobar, Á. Sánchez-Illana, J. Kuligowski, I. Torres-Cuevas, R. Solberg, H. T. Garberg, M.U. Huun, O.D. Saugstad, M. Vento, C. Cháfer-Pericás, Development of a reliable method based on ultra-performance liquid chromatography coupled to tandem mass spectrometry to measure thiol-associated oxidative stress in whole blood samples, J. Pharm. Biomed. Anal. 123 (2016) 104–112, https://doi.org/10.1016/j.jpba.2016.02.007.

[29] L. Torresano, F. Santacatterina, S. Domínguez-Zorita, C. Nuevo-Tapioles, A. Núñez-Salgado, P.B. Esparza-Moltó, L. González-Llorente, I. Romero-Carramiñana, C. Núñez de Arenas, B. Sánchez-Garrido, L. Nájera, C. Salas, M. Provencio, J. M. Cuezva, Analysis of the metabolic proteome of lung adenocarcinomas by reverse-phase protein arrays (RPPA) emphasizes mitochondria as targets for therapy, Oncogenesis 11 (2022), https://doi.org/10.1038/s41389-022-00400-y.

[30] F. Santacatterina, L. Torresano, A. Núñez-Salgado, P.B. Esparza-Molto, M. Olive, E. Gallardo, E. García-Arumi, A. Blazquez, A. González-Quintana, M.A. Martín, J. M. Cuezva, Different mitochondrial genetic defects exhibit the same protein signature of metabolism in skeletal muscle of PEO and MELAS patients: a role for oxidative stress, Free Radic. Biol. Med. 126 (2018) 235–248, https://doi.org/10.1016/j.freeradbiomed.2018.08.020.

[31] C. Martínez-Fernández De La Cámara, A.M. Hernández-Pinto, L. Olivares-González, C. Cuevas-Martín, M. Sánchez-Aragó, D. Hervás, D. Salom, J.M. Cuezva, E.J. De La Rosa, J.M. Millán, R. Rodrigo, Adalimumab reduces photoreceptor cell death in a mouse model of retinal degeneration, Sci. Rep. 5 (2015) 1–13, https://doi.org/10.1038/srep11764.

[32] X. Guo, G. Aviles, Y. Liu, R. Tian, B.A. Unger, Y.H.T. Lin, A.P. Wiita, K. Xu, M. A. Correia, M. Kampmann, Mitochondrial stress is relayed to the cytosol by an OMA1–DELE1–HRI pathway, Nature 579 (2020) 427–432, https://doi.org/10.1038/s41586-020-2078-2.

[33] G. Chidlow, J.P.M. Wood, B. Knoops, R.J. Casson, Expression and distribution of peroxiredoxins in the retina and optic nerve, Brain Struct. Funct. 221 (2016) 3903–3925, https://doi.org/10.1007/s00429-015-1135-3.

[34] P.J. Anderson, H. Watts, C. Hille, K. Philpott, P. Clark, M. Crocher, S. Gentleman, L.-S. Jen, Glial and endothelial blood-retinal barrier responses to amyloid-β in the neural retina of the rat, Clin. Ophthalmol. 2 (2008) 801, https://doi.org/10.2147/opth.s3967.

[35] N.D. Chinskey, C.G. Besirli, D.N. Zacks, Retinal cell death and current strategies in retinal neuroprotection, Curr. Opin. Ophthalmol. 25 (2014) 228–233, https://doi.org/10.1097/ICU.0000000000000043.

[36] G. Dvoriantchikova, K.R. Lypka, E.V. Adis, D. Ivanov, Multiple types of programmed necrosis such as necroptosis, pyroptosis, oxytosis/ferroptosis, and parthanatos contribute simultaneously to retinal damage after ischemia–reperfusion, Sci. Rep. 12 (2022) 1–15, https://doi.org/10.1038/s41598-022-22140-0.

[37] L. Sun, H. Wang, Z. Wang, S. He, S. Chen, D. Liao, L. Wang, J. Yan, W. Liu, X. Lei, X. Wang, Mixed lineage kinase domain-like protein mediates necrosis signaling downstream of RIP3 kinase, Cell 148 (2012) 213–227, https://doi.org/10.1016/j.cell.2011.11.031.

[38] A.L. Samson, Y. Zhang, N.D. Geoghegan, X.J. Gavin, K.A. Davies, M. J. Mlodzianoski, L.W. Whitehead, D. Frank, S.E. Garnish, C. Fitzgibbon, A. Hempel, S.N. Young, A.V. Jacobsen, W. Cawthorne, E.J. Petrie, M.C. Faux, K. Shield-Artin, N. Lalaoui, J.M. Hildebrand, J. Silke, K.L. Rogers, G. Lessene, E.D. Hawkins, J. M. Murphy, MLKL trafficking and accumulation at the plasma membrane control the kinetics and threshold for necroptosis, Nat. Commun. 11 (2020) 1–17, https://doi.org/10.1038/s41467-020-16887-1.

[39] J. Lewerenz, G. Ates, A. Methner, M. Conrad, P. Maher, Oxytosis/ferroptosis-(Re-) emerging roles for oxidative stress-dependent non-apoptotic cell death in diseases of the central nervous system, Front. Neurosci. 12 (2018), https://doi.org/10.3389/fnins.2018.00214.

[40] A. Anandhan, M. Dodson, C.J. Schmidlin, P. Liu, D.D. Zhang, Breakdown of an ironclad defense system: the critical role of NRF2 in mediating ferroptosis, Cell Chem. Biol. 27 (2020) 436–447, https://doi.org/10.1016/j.chembiol.2020.03.011.

[41] L. Baird, M. Yamamoto, The molecular mechanisms regulating the KEAP1-NRF2 pathway, Mol. Cell Biol. 40 (2020) 1–23, https://doi.org/10.1128/mcb.00099-20.

[42] P.A. Campochiaro, R.W. Strauss, L. Lu, G. Hafiz, Y. Wolfson, S.M. Shah, R. Sophie, T.A. Mir, H.P. Scholl, Is there excess oxidative stress and damage in eyes of patients with retinitis pigmentosa? Antioxidants Redox Signal. 23 (2015) 643–648, https://doi.org/10.1089/ars.2015.6327.

[43] S. Usui, B.C. Oveson, S.Y. Lee, Y. Jo, T. Yoshida, K. Miki, T. Iwase, L. Lu, P. A. Campochiaro, NADPH oxidase plays a central role in cone cell death in retinitis pigmentosa, J. Neurochem. 110 (2010) 1028–1037, https://doi.org/10.1111/j.1471-4159.2009.06195.x.NADPH.

[44] B.R. Cardoso, D.J. Hare, A.I. Bush, B.R. Roberts, Glutathione peroxidase 4: a new player in neurodegeneration? Mol. Psychiatr. 22 (2017) 328–335, https://doi.org/10.1038/mp.2016.196.

[45] L. Lu, B.C. Oveson, Y.J. Jo, T.W. Lauer, S. Usui, K. Komeima, B. Xie, P. A. Campochiaro, Increased expression of glutathione peroxidase 4 strongly protects retina from oxidative damage, Antioxidants Redox Signal. 11 (2009) 715–724, https://doi.org/10.1089/ars.2008.2171.

[46] Y. Liu, D. Wu, Q. Fu, S. Hao, Y. Gu, W. Zhao, S. Chen, F. Sheng, Y. Xu, Z. Chen, K. Yao, CHAC1 as a novel contributor of ferroptosis in retinal pigment epithelial cells with oxidative damage, Int. J. Mol. Sci. 24 (2023), https://doi.org/10.3390/ijms24021582.

[47] P. Ahuja-Jensen, S. Johnsen-Soriano, S. Ahuja, F. Bosch-Morell, M. Sancho-Tello, F. J. Romero, M. Abrahamson, T. Van Veen, Low glutathione peroxidase in rd1 mouse retina increases oxidative stress and proteases, Neuroreport 18 (2007) 797–801, https://doi.org/10.1097/WNR.0b013e3280c1e344.

[48] Y. Ozawa, Oxidative stress in the light-exposed retina and its implication in age-related macular degeneration, Redox Biol. 37 (2020), 101779, https://doi.org/10.1016/j.redox.2020.101779.

[49] A. Garanto, M. Riera, E. Pomares, J. Permanyer, M. de Castro-Miró, F. Sava, J. F. Abril, G. Marfany, R. Gonzàlez-Duarte, High transcriptional complexity of the retinitis pigmentosa CERKL gene in human and mouse, Invest. Ophthalmol. Vis. Sci. 52 (2011) 5202–5214, https://doi.org/10.1167/iovs.10-7101.

[50] A. Noailles, V. Maneu, L. Campello, P. Lax, N. Cuenca, Systemic inflammation induced by lipopolysaccharide aggravates inherited retinal dystrophy, Cell Death Dis. 9 (2018), https://doi.org/10.1038/s41419-018-0355-x.

[51] B.W. Jones, R.E. Marc, Retinal remodeling during retinal degeneration, Exp. Eye Res. 81 (2005) 123–137, https://doi.org/10.1016/j.exer.2005.03.006.

[52] N. Martínez-Gil, V. Maneu, O. Kutsyr, L. Fernández-Sánchez, X. Sánchez-Sáez, C. Sánchez-Castillo, L. Campello, P. Lax, I. Pinilla, N. Cuenca, Cellular and molecular alterations in neurons and glial cells in inherited retinal degeneration, Front. Neuroanat. 16 (2022) 1–18, https://doi.org/10.3389/fnana.2022.984052.

[53] Z. Yu, V.S.M.C. Correa, N.E. Efstathiou, H. Albertos-Arranz, X. Chen, K. Ishihara, Y. Iesato, T. Narimatsu, D. Ntentakis, D.G. Vavvas, UVA induces retinal photoreceptor cell death via receptor interacting protein 3 kinase mediated necroptosis, Cell Death Dis. 8 (2022) 1–11, https://doi.org/10.1038/s41420-022-01273-1.

[54] Y. Tian, J. Lu, X. Hao, H. Li, G. Zhang, X. Liu, X. Li, C. Zhao, W. Kuang, D. Chen, M. Zhu, FTH1 inhibits ferroptosis through ferritinophagy in the 6-OHDA model of Parkinson's disease, Neurotherapeutics 17 (2020) 1796–1812, https://doi.org/10.1007/s13311-020-00929-z.

[55] W. Shu, B.H. Baumann, Y. Song, Y. Liu, X. Wu, J.L. Dunaief, Ferrous but not ferric iron sulfate kills photoreceptors and induces photoreceptor-dependent RPE autofluorescence, Redox Biol. 34 (2020), 101469, https://doi.org/10.1016/j.redox.2020.101469.

[56] J. Sancho-Pelluz, B. Arango-Gonzalez, S. Kustermann, F.J. Romero, T. Van Veen, E. Zrenner, P. Ekström, F. Paquet-Durand, Photoreceptor cell death mechanisms in inherited retinal degeneration, Mol. Neurobiol. 38 (2008) 253–269, https://doi.org/10.1007/s12035-008-8045-9.

[57] W. Xiong, A.E.M.C. Garfinkel, Y. Li, L.I. Benowitz, C.L. Cepko, NRF2 promotes neuronal survival in neurodegeneration and acute nerve damage, J. Clin. Invest. 125 (2015) 1433–1445, https://doi.org/10.1172/JCI79735.